



RESEARCH MEMORANDUM

JET EFFECTS ON THE DRAG OF CONICAL AFTERBODIES

FOR MACH NUMBERS OF 0.6 TO 1.28

By James M. Cabbage, Jr.

Langley Aeronautical Laboratory
Langley Field, Va.

**NATIONAL ADVISORY COMMITTEE
FOR AERONAUTICS
WASHINGTON**

April 12, 1957
Declassified May 29, 1959

NATIONAL ADVISORY COMMITTEE FOR AERONAUTICS

RESEARCH MEMORANDUM

JET EFFECTS ON THE DRAG OF CONICAL AFTERBODIES

FOR MACH NUMBERS OF 0.6 TO 1.28

By James M. Cabbage, Jr.

SUMMARY

An investigation has been conducted at Mach numbers from 0.6 to 1.28 to determine the drag characteristics of a series of conical afterbodies with a cold sonic jet issuing from the base. The models investigated had boattail angles from 3° to 45° with ratios of the jet diameter to the base diameter of 0.65 and 0.75; values of the ratios of the base diameter to the maximum diameter were 0.55, 0.70, and 0.85. The jet total-pressure ratio ranged from the no-jet-flow condition to approximately 8.

The results show that the boattail angle for minimum afterbody drag at subsonic speeds was in the 5° to 8° range and between approximately 2.5° and 5° at supersonic speeds. These values of boattail angle were not altered significantly over the range of jet pressure ratios investigated. The pressure ratio of the jet did, however, influence the level of the minimum drag coefficient. The afterbody drag coefficients of a 30° and 45° boattailed body were equal to or greater than that of a cylindrical afterbody for certain test conditions. In general, the afterbody drag coefficient increased as the ratio of the base diameter to the maximum diameter increased at both subsonic and supersonic speeds.

INTRODUCTION

Present-day jet-propelled aircraft capable of supersonic flight cruises at high subsonic speeds in order to achieve a significant operating range. Since afterburner operation is not required for the cruise condition, the exit area of the nozzle must be reduced to maintain propulsive efficiency. The reduction in nozzle exit area necessitates increased boattailing of the afterbody or a larger base annulus. These changes in the shape of the afterbody can result in lower static pressures; thus, the drag of the afterbody increases and the range capabilities of the aircraft reduces.

The investigation reported herein is part of a study to determine the effects of a propulsive jet on the drag of the afterbody from which it issues through the speed range from subsonic to supersonic speeds. The initial part of this study was concerned with jet effects on a cylindrical afterbody and is described in reference 1. The work of reference 2 and the present investigation were conducted concurrently and the conical afterbody configurations of the former are geometrically similar to the configurations of this investigation. Studies by other researchers have been conducted at transonic speeds and some of these are reported in references 3 to 6. Reference 3 presents data on conical and contoured afterbodies obtained in a perforated tunnel in addition to results from a study of boundary-layer and tunnel-wall effects on the data. Reference 6 is one of several reported studies of jet effects on the afterbody of rocket-launched free-flight models.

The present investigation was conducted in the Langley internal aerodynamics laboratory over a Mach number range of 0.6 to 1.28 at corresponding Reynolds number of 3.4×10^6 to 4.8×10^6 per foot. The conical afterbodies investigated had boattail angles of 3° , 5.6° , 8° , 16° , 30° , and 45° with ratios of the jet diameter to the base diameter of 0.65 and 0.75. Values of the ratio of the base diameter to the maximum diameter of these models were 0.55, 0.70, and 0.85. The jet total-pressure ratio was varied from no jet flow to approximately 8 and the stagnation temperature of the issuing jet was approximately 70° F.

SYMBOLS

A area

$C_{D,\beta}$ boattail drag coefficient, $\int_1^{(r_b/r_m)^2} - C_{p,\beta} d\left(\frac{r_x}{r_m}\right)^2$

$C_{D,b}$ base drag coefficient, $-C_{p,b} \frac{A_b - A_j}{A_m}$

$C_{D,a}$ afterbody drag coefficient, $C_{D,\beta} + C_{D,b}$

C_p pressure coefficient, $\frac{\frac{p}{p_\infty} - 1}{\frac{\gamma}{2} M_\infty^2}$

d	diameter
H	total pressure
M	Mach number
p	static pressure
u	velocity of flow at distance y from model support tube and parallel to tunnel center line
U_{∞}	free-stream velocity
r	radius
x	distance along center line of model from juncture of afterbody and model support tube
y	perpendicular distance from model support tube
δ	boundary-layer thickness
β	boattail angle; angle between center line and a generatrix of model
γ	ratio of specific heats

Subscripts:

a	afterbody
b	base
m	maximum
j	jet
β	boattail
∞	free stream
x	local
o	stagnation

Unless otherwise stated, "base diameter ratio" and "jet diameter ratio" will hereinafter refer to the ratio of the base diameter to the

maximum diameter and ratio of the jet diameter to the base diameter. In addition, "jet pressure ratio" will refer to the ratio of the jet total pressure to the stream static pressure.

APPARATUS AND METHODS

A drawing of the tunnel used in this investigation is presented as figure 1. This tunnel is the same facility employed in the investigation reported in reference 1 and is described in detail in that reference. A minor modification at the rear of the test section (at the conclusion of the tests of ref. 1) increased the cross-sectional area of the test section at this point and, in turn, increased the maximum Mach number of the tunnel by about 0.04. The stream stagnation temperature at the maximum Mach number was approximately 180° F.

The model support arrangement shown in figure 1 is also identical to the one described in reference 1. The forward strut was used to duct high-pressure air to the model support tube and the two lower struts contained all pressure leads from the model. The jet air was supplied from three 1,000-cubic-foot tanks which were pressurized to approximately 100 pounds per square inch. Pneumatically operated valves were used to maintain a constant pressure at the entrance of the jet nozzle. The temperature of the air supplied to the jet nozzle was approximately 70° F.

A sketch of a typical model is presented in figure 2(a) and a photograph of 11 of the 22 models tested is presented as figure 2(b). The boattail angle β was varied from 30° to 45°; the base diameter ratios were 0.55, 0.70, and 0.85. Static-pressure orifices 0.020 inch in diameter were installed along a meridian of the afterbody. The shortest afterbody contained five boattail static orifices, whereas the longest model had 11. Two 0.020-inch-diameter base-pressure orifices were installed 0.09 inch from the edge of the base on each model; one orifice was in line with the boattail orifices and the second was located 90° counterclockwise from the first (see fig. 2(a)). A single 0.020-inch-diameter orifice was located 0.375 inch upstream from the cone-cylinder juncture on all models and was in line with the boattail orifices.

The shape of the sonic nozzle was identical for all the models and consisted of a 10°-included-angle convergence section followed by a constant-diameter portion 0.2 inch in length. Jet diameters of 1.3 and 1.5 inches were used in this investigation. All models were installed in the test section with the line of boattail orifices in a vertical plane through the center line of the model and opposite the slotted top wall of the test section.

A 0.040-inch-diameter total-pressure probe was used to obtain total-pressure distributions across the vertical diameter of the jet. The end of the probe passed within 0.015 inch of the base of the model, and the pressure was continuously recorded by a three-variable recording potentiometer.

All static pressures were recorded photographically from a multiple-tube manometer containing tetrabromoethane. Boattail pressure coefficients were mechanically integrated for each test condition to obtain boattail drag coefficients. The base drag coefficients, jet on and off, were computed using the area of the base annulus only. The boundary layer on the model support pipe was assumed to be the same as that reported in reference 1 since the apparatus was identical. Figure 6(b) of reference 1 is reproduced as figure 3 in the present report; this figure shows that the boundary layer was fully turbulent at a point 5.5 inches upstream of the base. The boundary-layer thickness at this point was approximately 0.4 inch or 20 percent of the maximum model diameter.

RESULTS AND DISCUSSION

Afterbody Pressure Distributions

A typical pressure distribution over a conical afterbody at $M_\infty = 0.9$ and at a jet pressure ratio of 4 is shown in figure 4. A schlieren photograph of the model at these test conditions is shown at the top of the figure. Although this distribution is for a particular model operating at specific test conditions, it is representative of those obtained for other models at other test conditions. The rapid acceleration of the flow at the cone-cylinder juncture is noted as well as the extent to which this acceleration affects the pressures upstream of the juncture. The pressure coefficient corresponding to the static pressure necessary for sonic flow along the model is indicated by an arrow on the ordinate at $\frac{x}{d_m} = -0.4$. As the flow proceeds along the afterbody it compresses rapidly and reaches above ambient pressures near the base. As the boattail angle increases, the pressures near the juncture become more negative until the angle becomes large enough to cause separation of the flow from the afterbody at this point. Separation of the flow at the cone-cylinder juncture is characterized by relatively small negative pressure coefficients at the juncture and a distribution which is nearly constant over the length of the afterbody. Except for a region close to the base, a distribution for unseparated flow is affected very little by increasing the base diameter ratio (smaller afterbody length) at a constant boattail angle. At high jet pressure

ratios the interference between the jet and external flow causes higher pressures on the base and this influences the pressures on the afterbody for a short distance upstream of the base. Effects similar to those noted also occurred at supersonic speeds. The compression of the flow over the boattail, however, was more gradual at supersonic speeds than at subsonic speeds.

Detail afterbody pressure-coefficient distributions for models with a jet diameter ratio of 0.65 (except the $\beta = 45^\circ$ model) are presented in figure 5. The last boattail pressure orifice on all models was located 0.40 inch ($x/d_m = 0.02$) upstream of the base; the end point for all curves is the base pressure coefficient. Schlieren photographs of the flow field about four afterbody configurations at several values of jet pressure ratio and Mach number are shown in figure 6. The distributions for the $\beta = 45^\circ$ model were essentially the same as those for the 30° model and are, therefore, not shown. For the latter, the distributions shown in figures 5(b) and (c) and the schlieren photographs in figure 6(d) show that the flow separates completely at the cone-cylinder juncture. It will also be noted that the base pressure coefficient is nearly the same as the average boattail pressure coefficient. The value of this coefficient is approximately equal to the pressure measured at the base of a cylindrical model with the same ratio of jet diameter to model diameter. (See ref. 1.)

The effect of the relatively thick boundary layer on the results of this investigation has not been experimentally determined. However, work by other researchers (refs. 3 and 4) shows that variation in δ/d_m from 0.05 to 0.184 did not significantly affect the base pressure or boattail drag coefficients. In reference 3, δ/d_m was varied from 0.07 to 0.184 at transonic speeds and at $M = 1.5$ for a series of boattailed afterbodies. In reference 4, δ/d_m was varied from 0.05 to 0.18 at $M = 2.0$ for a cylindrical afterbody. The tunnel-wall interference effects are also thought to be small with the possible exception of the range between $M_\infty = 1.0$ and 1.1. It was pointed out in reference 1 that significant wall effects may be present at $M_\infty = 1.0$ because of the very low pressure existing on the base of the cylindrical afterbody. Base pressures of the magnitude reported in reference 1 were not encountered in the present investigation but very low pressures did occur at the cone-cylinder juncture of the $\beta = 8^\circ$ and 16° model at $M_\infty = 1.0$. This expansion may be reflected from the tunnel wall as a further expansion at $M_\infty = 1.0$ and, thus, influences the pressures on the afterbody, especially for the case of the longer models. At $M_\infty = 1.10$ the schlieren photographs of figure 6 show that the expansion wave originating at the cone-cylinder juncture is inclined at a rather large angle with respect to the direction of the free-stream flow, and its reflection

from the tunnel wall intersects the model wake some distance downstream of the model. Although tunnel-wall interference effects may be present at $M_\infty = 1.0$ to about $M_\infty = 1.1$, it is felt that the order of magnitude and the trend of the coefficients are valid throughout the speed range of these tests.

Afterbody Drag

Basic data.- Boattail ($C_{D,\beta}$), base ($C_{D,b}$), and afterbody drag coefficients ($C_{D,a}$) are presented as a function of jet pressure ratio at constant values of Mach number in figures 7 and 8. All configurations in figure 7 have a jet diameter ratio of 0.65 and those in figure 8 have a jet diameter ratio of 0.75.

Although the boattail drag coefficient for the $\beta = 3^\circ$ model, figure 7(a), is low and nearly independent of Mach number and jet pressure ratio, both of these parameters have a substantial effect on the base drag coefficient. The base drag coefficient at supersonic speeds peaks sharply at a jet pressure ratio of 2 but at $M_\infty \leq 1.0$ reached a maximum between a jet pressure ratio of 3 and 4. Since the boattail drag was small and unaffected by Mach number and jet pressure ratio, the afterbody drag coefficient followed the same variation with these parameters as did the base drag coefficient.

Increasing the boattail angle to 5.6° , figure 7(b), caused the boattail drag coefficient to increase and the base drag coefficient to decrease resulting in an afterbody drag coefficient for a base diameter ratio of 0.85 that was very little different from that obtained at $\beta = 3^\circ$. As in the case for the 3° model, the maximum afterbody drag coefficient at supersonic speeds occurred at a jet pressure ratio of 2 and at Mach numbers equal to or less than 1.0 between 3 and 4. Decreasing the base diameter ratio to 0.70, figure 7(c), increased the boattail drag coefficient slightly at supersonic Mach numbers and reduced the base drag coefficient substantially throughout the Mach number range of these tests. Thrust was experienced on the base at jet pressure ratios above about 5.5. The decrease in the base drag coefficient is due in part to the reduced base annulus area which for the longer afterbody was about 68 percent of that for the shorter model. The reduction in afterbody drag coefficient due to reduced base diameter ratio was small at jet pressure ratios of 6 or greater.

Increasing the boattail angle to 8° , figure 7(d), caused a further increase in the boattail drag coefficient. In general, the base drag coefficient increased slightly at supersonic speeds and decreased at sonic and subsonic speeds over the jet-pressure-ratio range. It will be noted in figures 7(a) to 7(e) at supersonic speeds that the base and

afterbody drag coefficients of a longer body do not reach a maximum peak as rapidly as the coefficients for a shorter body.

The $\beta = 16^\circ$ model, figures 7(f), (g), and (h), was the only model tested at all three base diameter ratios. This greater degree of boat-tailing increased the afterbody drag coefficient substantially above that for the models with lower boattail angles at supersonic speeds. Decreasing the base diameter ratio from 0.85, figure 7(f), to 0.70 and 0.55, figures 7(g) and (h), respectively, caused a substantial decrease in the base drag coefficient with essentially zero drag or thrust (negative drag coefficient) experienced for the longer afterbody over the entire Mach number and jet-pressure-ratio range. The greatest effect of the jet on the afterbody drag coefficient occurred for the shorter model while the least effect occurred for the longer model.

Between boattail angles of 16° and 30° , the external flow separates completely from the model and the pressures acting upon the boattail and base are nearly constant for a fixed operating condition. Therefore, the values of the base and boattail drag coefficients of figures 7(i), (j), and (k) are primarily dependent upon the projected areas of the base and boattail. For the 30° model in figures 7(i) and (j), the effect of jet pressure ratio on the afterbody drag coefficient differed as the base diameter ratio decreased. The afterbody drag coefficient tended to reach a maximum at a higher jet pressure ratio for the longer model. (See fig. 7(j).) If the 30° and 45° models are considered to be similar to a cylindrical afterbody, this trend is in agreement with the results of reference 1 where it was shown that the jet size had a strong effect on the base pressure. With the smaller diameter jet the beneficial jet-interference effects are delayed until large jet pressure ratios are reached.

Increasing the jet diameter ratio to 0.75 for the range of boattail angles tested, figure 8, had a general effect of reducing the drag of the afterbody. The boattail drag coefficient was not noticeably affected by the increase in jet diameter ratio except at the higher jet pressure ratios. The reduction in the base drag coefficient at jet pressure ratios of 2 and 3 and at all Mach numbers was less than that which would occur due to the reduced area of the base annulus. At the higher jet pressure ratios this decrease in base drag was, in general, greater than that due to the smaller base size.

Effect of boattail angle.- Part of the basic data shown in figures 7 and 8 is presented again in figures 9 and 10 in the form of afterbody and boattail drag coefficients as a function of boattail angle at several values of Mach number and jet pressure ratio. Figure 9 is for a jet diameter ratio of 0.65 and figure 10 is for a jet diameter ratio of 0.75.

For a base diameter ratio of 0.85, figure 9(a), the boattail angle has very little effect on the afterbody drag coefficient at $M_\infty = 0.6$. At a Mach number of 0.9, however, the afterbody drag coefficient reaches a minimum at $\beta \approx 8^\circ$ and increases rapidly at boattail angles greater than this value. A small increase in the afterbody drag coefficient occurs as the boattail angle is reduced below this value. At a Mach number of 1.2 the afterbody drag coefficient tends to reach a minimum at a boattail angle of approximately 3° . These optimum values of boattail angle are in agreement with the optimum values observed in reference 2. The boattail drag coefficient increased almost linearly with increasing boattail angle at both subsonic and supersonic speeds for this base diameter ratio. As the boattail angle increases, the expansion of the flow around the cone-cylinder juncture also increases and causes the local pressures to decrease. Thus, the boattail drag coefficient increases with boattail angle. It will be noted that jet pressure ratio influences the level of the minimum afterbody drag coefficient but not the value of boattail angle at which the minimum occurs and, also, that jet pressure ratio has little or no effect on the boattail drag coefficient for this value of base diameter ratio.

Decreasing the base diameter ratio to 0.70, figure 9(b), causes the boattail angle to have a slightly greater effect on afterbody drag coefficient at a Mach number of 0.6. The optimum value of boattail angle at this speed depends to some extent upon jet pressure ratio. The boattail angle for minimum afterbody drag coefficient at $M_\infty = 0.9$ is in the range between 6° and 9° . Except for the highest jet pressure ratio, the drag coefficient of the complete afterbody is about the same at boattail angles of 16° and 30° . Increasing the Mach number to supersonic speeds at this base diameter ratio shifts the optimum boattail angle to less than 5° as in the case for the shorter afterbody of figure 9(a). Also, as in the case for the shorter afterbody, jet pressure ratio does not influence the optimum boattail angle. At both subsonic and supersonic speeds, the drag of the 16° and 30° models is about the same as that for a cylindrical afterbody. The boattail drag coefficient at subsonic speeds increases with boattail angle up to 16° and is approximately constant from this value to a boattail angle of 30° . This would be expected since the flow separates from the model at a boattail angle somewhat greater than 16° . At supersonic speeds, the data show the boattail drag for the large-angle boattailed models to be somewhat less than for the models with smaller boattail angles. This is also true for the afterbody drag at the jet operating conditions shown at $M_\infty = 1.2$. These data indicate that complete separation of the flow from an afterbody with a large boattail angle may be desirable at supersonic speeds for minimum drag provided that the base area is small. Otherwise, the jet would tend to aspirate the base and increase the afterbody drag above that for smaller boattail angles.

The effect of large boattail angles on afterbody and boattail drag at a base diameter ratio of 0.55 is shown in figure 9(c). At subsonic speeds, the afterbody drag coefficient at the two large boattail angles is about equal for all jet pressure ratios shown except at a jet pressure ratio of 6. At this pressure ratio the aspirating effect of the jet is probably greater on the $\beta = 45^\circ$ model. The boattail drag coefficient at these Mach numbers follows about the same trend as the afterbody drag coefficient. At supersonic speeds the boattail drag coefficient shows the same trend for $\beta = 30^\circ$ as observed for the larger base diameter ratio. (See fig. 9(b).) The afterbody drag coefficient, however, increases steadily as the boattail angle increases from 16° at the higher jet pressure ratios. For the no-jet-flow condition at this Mach number, the afterbody drag coefficient is nearly constant from a boattail angle of 16° to a boattail angle of 30° . Plotting these data of figure 9(c) along with those of figures 9(a) and (b) on a common plot for a given jet pressure ratio and Mach number shows that the optimum boattail angle for a base diameter ratio of 0.55 would be about the same as previously observed for the two larger base diameter ratios. That is, the data of figure 9(c) tend to fair into the data of figure 9(b) at $\beta = 16^\circ$.

Essentially the same trends noted for the data of figure 9 (jet diameter ratio of 0.65) occurred for the data of figure 10 where the jet diameter ratio was 0.75. The optimum boattail angle for this jet diameter ratio at both subsonic and supersonic speeds appears to be shifted 2° or 3° toward a smaller angle. This is reasonable in that the jet and external flows are in closer proximity to each other with the larger jet diameter.

Effect of base diameter ratio.- Portions of the data presented in figures 7 and 8 have also been replotted to emphasize the variation of afterbody and boattail drag coefficient with base diameter ratio. These cross plots are presented in figures 11 and 12 for boattail angles of 5.6° , 8° , and 16° . Figure 11 is for a jet diameter ratio of 0.65 and figure 12 for a jet diameter ratio of 0.75. Since the jet diameter ratio is a constant in figure 11 and in figure 12, the diameter of the jet relative to the maximum diameter of the model decreases with the base diameter ratio.

The effect of base diameter ratio on the afterbody drag coefficient was approximately the same for all three boattail angles and depended primarily upon the operating conditions of the jet. This influence of the jet upon the effect of base diameter ratio was greatest at supersonic speeds. In general, however, the afterbody drag coefficient increased with increasing base diameter ratio primarily because of the greater contribution of the base drag to the total drag of the afterbody. The boattail drag coefficient decreased with increasing base

diameter ratio with the largest decrease occurring at supersonic speeds. At a Mach number of 0.6, the boattail drag coefficient was essentially constant for the range of base diameter ratios investigated. The data of figures 11 and 12 point out the need for a short afterbody (large base diameter ratio) to realize minimum boattail drag for a particular boattail angle; however, large base diameter ratios result in large base areas which can cause large base drag penalties. Long afterbodies allow the external flow to compress to a higher pressure along the afterbody and, thus, help to increase the pressure acting on the base, but for some configurations the increased boattail drag may offset any reduction in base drag.

Comparison with other data.- Figure 13 presents a comparison of data from references 2 and 3 with results from the present investigation. The data are for a 15° boattailed afterbody with a base diameter ratio and jet diameter ratio of 0.75. In neither reference 2 or the present investigation were models with $\beta = 15^\circ$ and $d_b/d_m = 0.75$ tested so that the basic data were interpolated from several crossplots to obtain afterbody drag coefficients for this comparison. Model 1 of reference 3 had a tunnel blockage of 3.1 percent; reference 2 and the present investigation had blocked areas of 3.88 and 3.08 percent, respectively. Data for model 1 of reference 3 at a wall convergence angle of 0.5° were chosen since it was reported that the most uniform Mach number distribution of the empty tunnel was obtained at this wall setting.

Some difference exists between the magnitude of $C_{D,a}$ for the present work and that of reference 3 at the no-jet-flow condition. This is thought to be due largely to extending the data of reference 3 to the no-jet-flow condition by simply fairing the curves to $H_j/p_\infty = 1.0$. It will be noted in the basic data curves of figures 7 and 8 that at subsonic speeds $C_{D,a}$ for $\beta = 16^\circ$ tends to increase abruptly between no jet flow and $H_j/p_\infty = 1.5$. At a jet pressure ratio of 5, the present data and that of reference 3 are in good agreement throughout the Mach number range of these tests.

SUMMARY OF RESULTS

An experimental investigation at Mach numbers of 0.6 to 1.28 of jet effects on the drag of a series of conical afterbodies yielded the following results:

1. At high subsonic speeds, the boattail angle for minimum afterbody drag coefficient was in the range between 5° and 8° . At supersonic

speeds, the optimum value of boattail angle was in the range from approximately 2.5° to 5° .

2. Optimum values of boattail angles were not altered significantly over the range of jet pressure ratios investigated. The pressure at which the jet operated did, however, influence the level of the minimum drag coefficient.

3. The presence of the jet was unfavorable on afterbody drag, except at jet pressure ratios of about 6 or greater, and the variation of afterbody drag with jet pressure ratio decreased as the ratio of the base diameter to the maximum diameter decreased.

4. For the 30° and 45° boattailed bodies, the pressures over the boattail were about constant and equal to the base pressure due to complete separation of the flow from the model. The afterbody drag coefficient of these models was approximately equal to or greater than the base drag coefficient of a cylindrical afterbody.

5. At subsonic speeds, the effect of the ratio of the base diameter to the maximum diameter on afterbody drag coefficient was small; at supersonic speeds, the effect depended to a large extent upon the jet-total-pressure ratio. In general, the base drag coefficient decreased as the ratio of the base diameter to the maximum diameter decreased.

Langley Aeronautical Laboratory,
National Advisory Committee for Aeronautics,
Langley Field, Va., February 8, 1957.

REFERENCES

1. Cabbage, James M., Jr.: Jet Effects on Base and Afterbody Pressures of a Cylindrical Afterbody at Transonic Speeds. NACA RM L56C21, 1956.
2. Silhan, Frank V., and Cabbage, James M., Jr.: Drag of Conical and Circular-Arc Boattail Afterbodies at Mach Numbers From 0.6 to 1.3. NACA RM L56K22, 1957.
3. Pel, C., and Rustemeyer, A.: Investigation of Turbojet Exhaust-Interference Drag. Rep. R-0801-12, United Aircraft Corp. Res. Dept., Nov. 1955.
4. Cortright, Edgar M., Jr., and Kochendorfer, Fred D.: Jet Effects on Flow Over Afterbodies in Supersonic Stream. NACA RM E53H25, 1953.
5. Henry, Beverly, Jr., and Cahn, Maurice S.: Preliminary Results of an Investigation at Transonic Speeds To Determine the Effects of a Heated Propulsive Jet on the Drag Characteristics of a Related Series of Afterbodies. NACA RM L55A24a, 1955.
6. Falanga, Ralph A.: A Free-Flight Investigation of the Effects of Simulated Sonic Turbojet Exhaust on the Drag of a Boattail Body With Various Jet Sizes From Mach Number 0.87 to 1.50. NACA RM L55F09a, 1955.

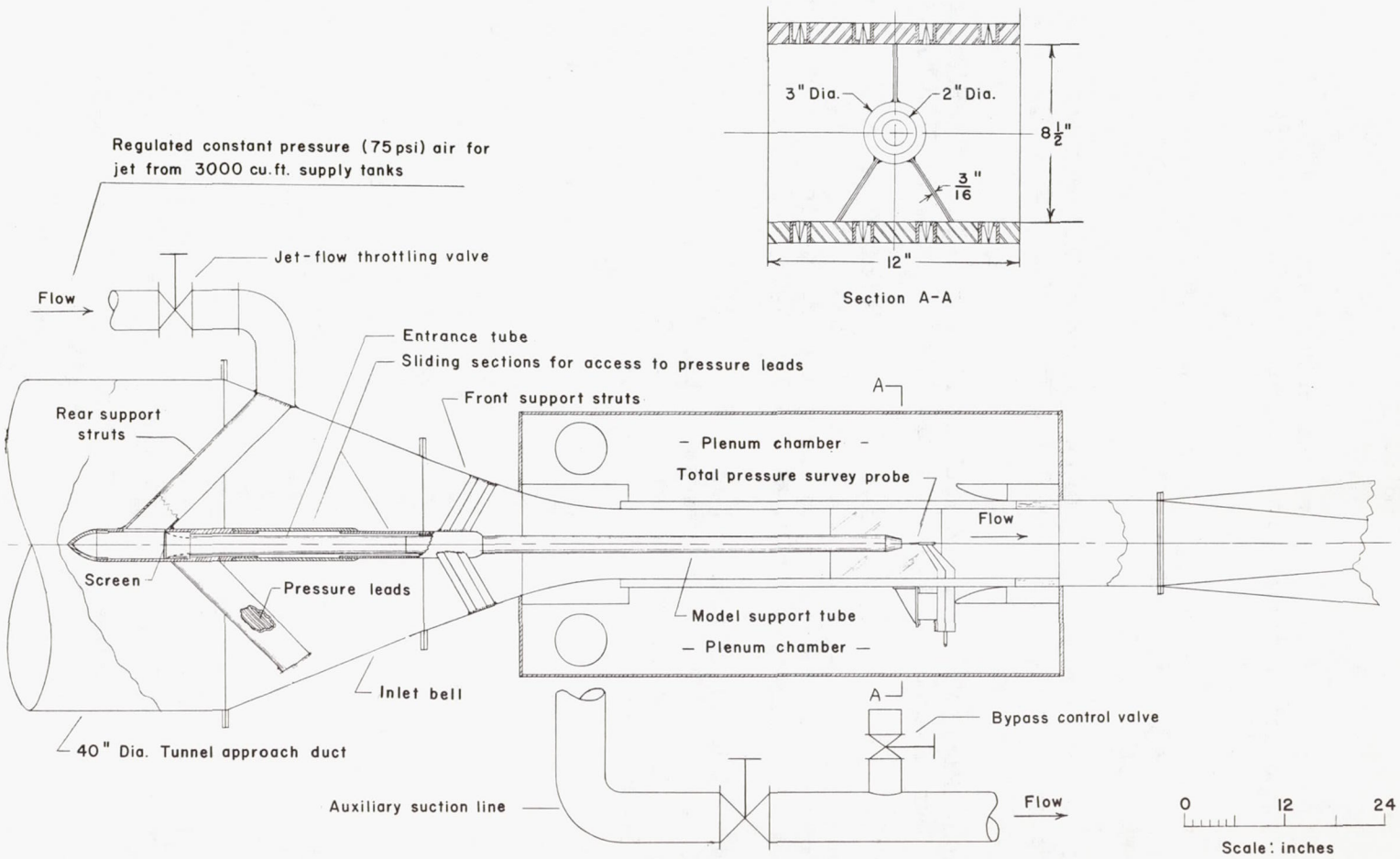
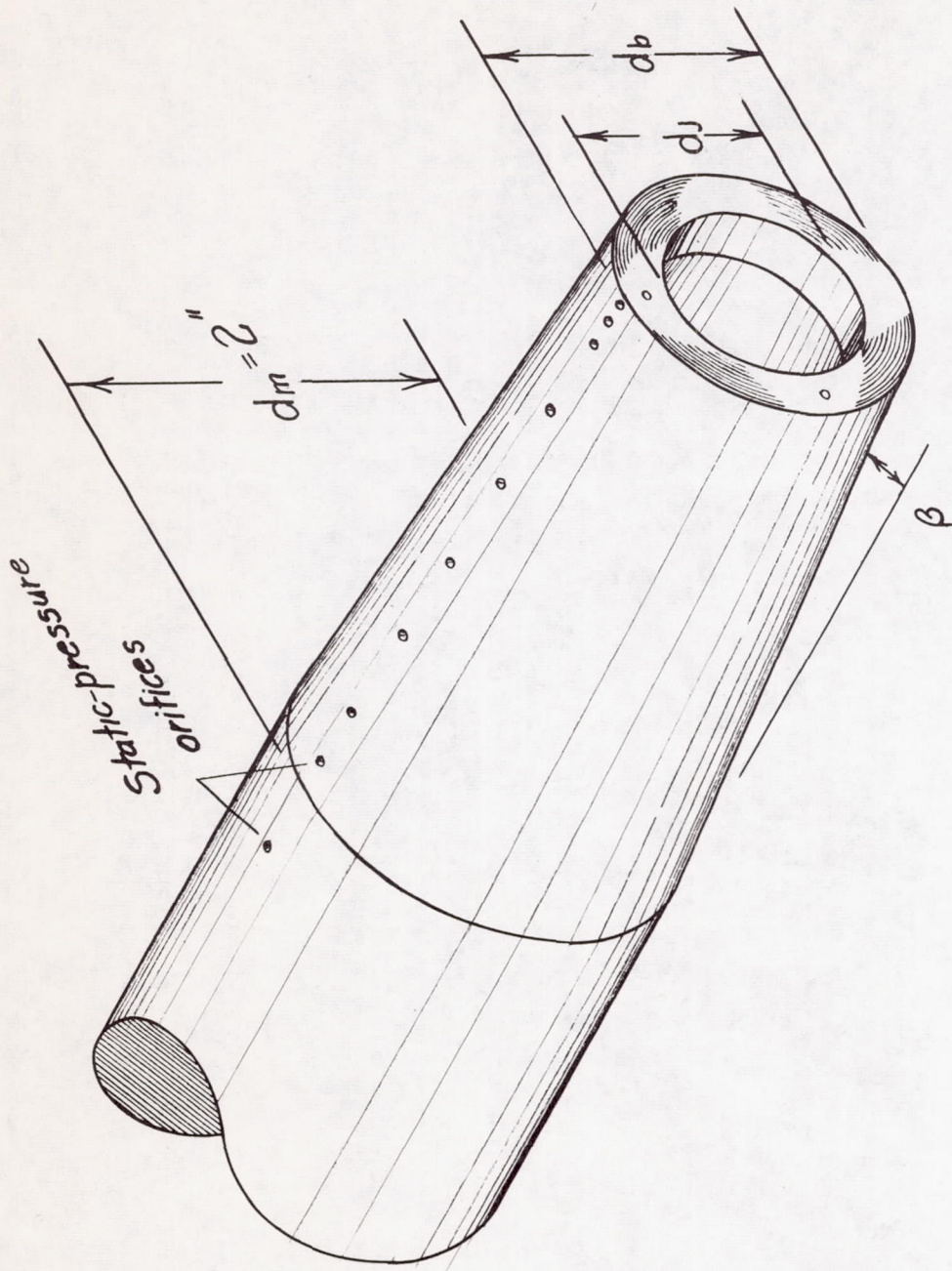
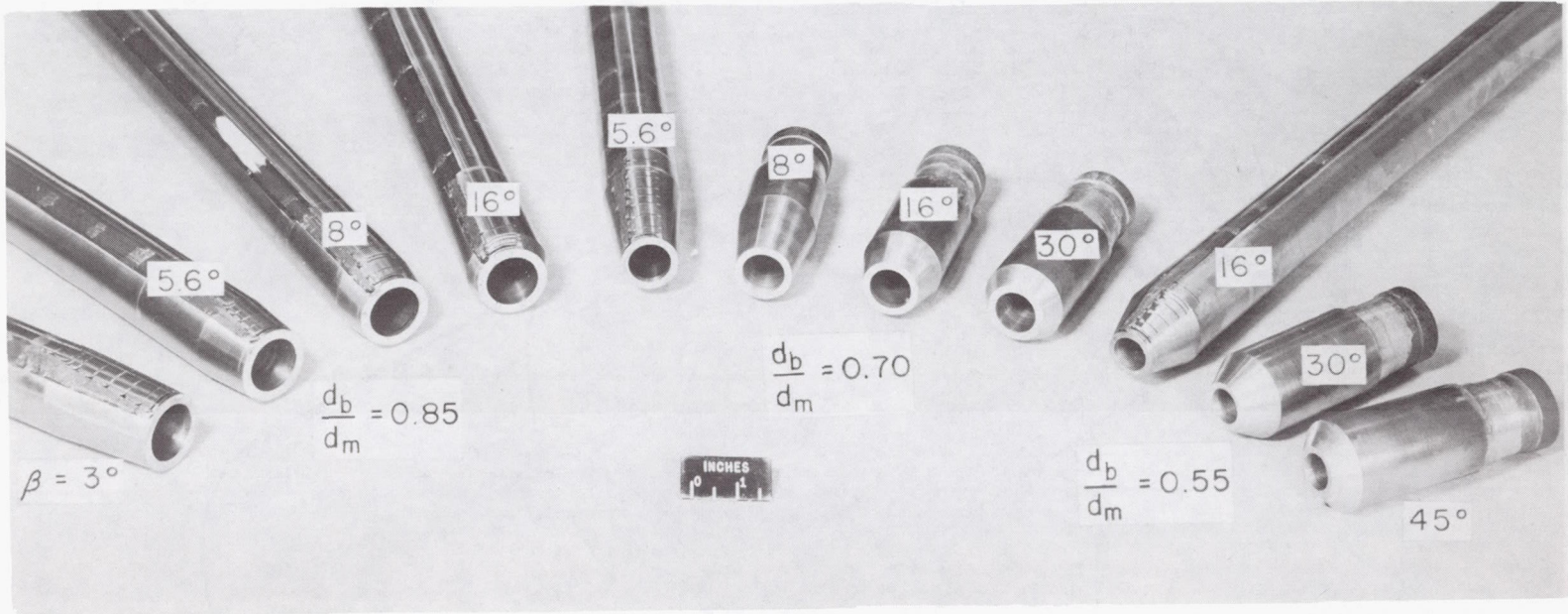


Figure 1.- Drawing of tunnel showing model support arrangement.



(a) Sketch of typical model.

Figure 2.- Afterbody model configurations.



(b) Afterbody models. $d_j/d_b = 0.75$.

L-94073.1

Figure 2.- Concluded.

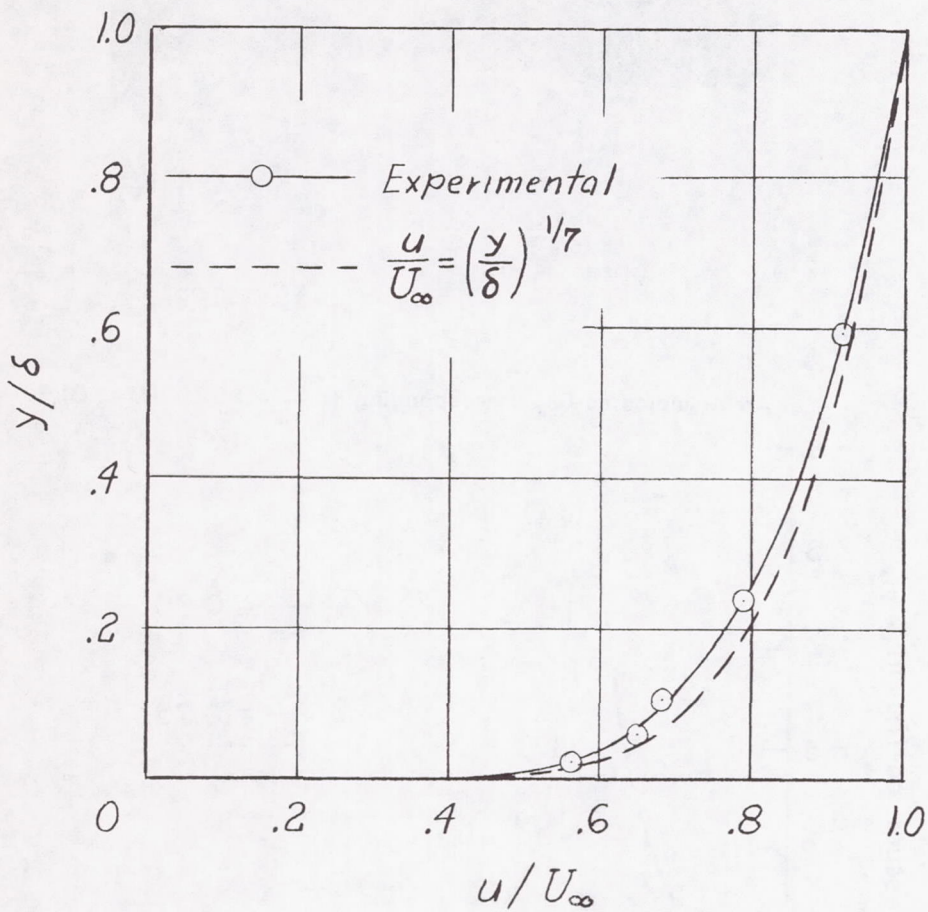
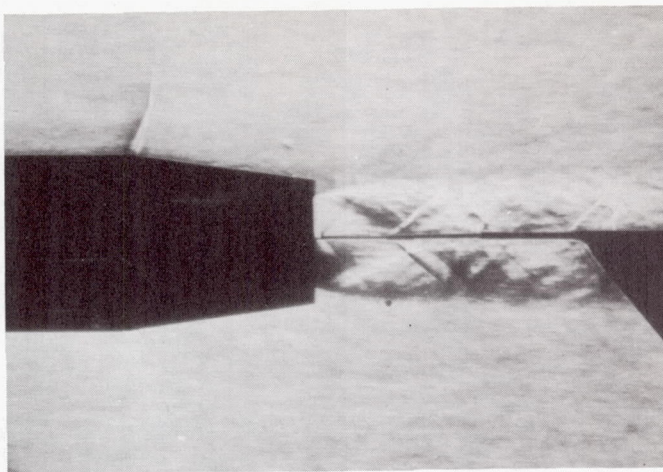


Figure 3.- Comparison of boundary-layer profile 5.5 inches upstream from the base of a cylindrical afterbody and at $M_\infty = 0.9$ with a 1/7 power profile (ref. 1).



L-57-172

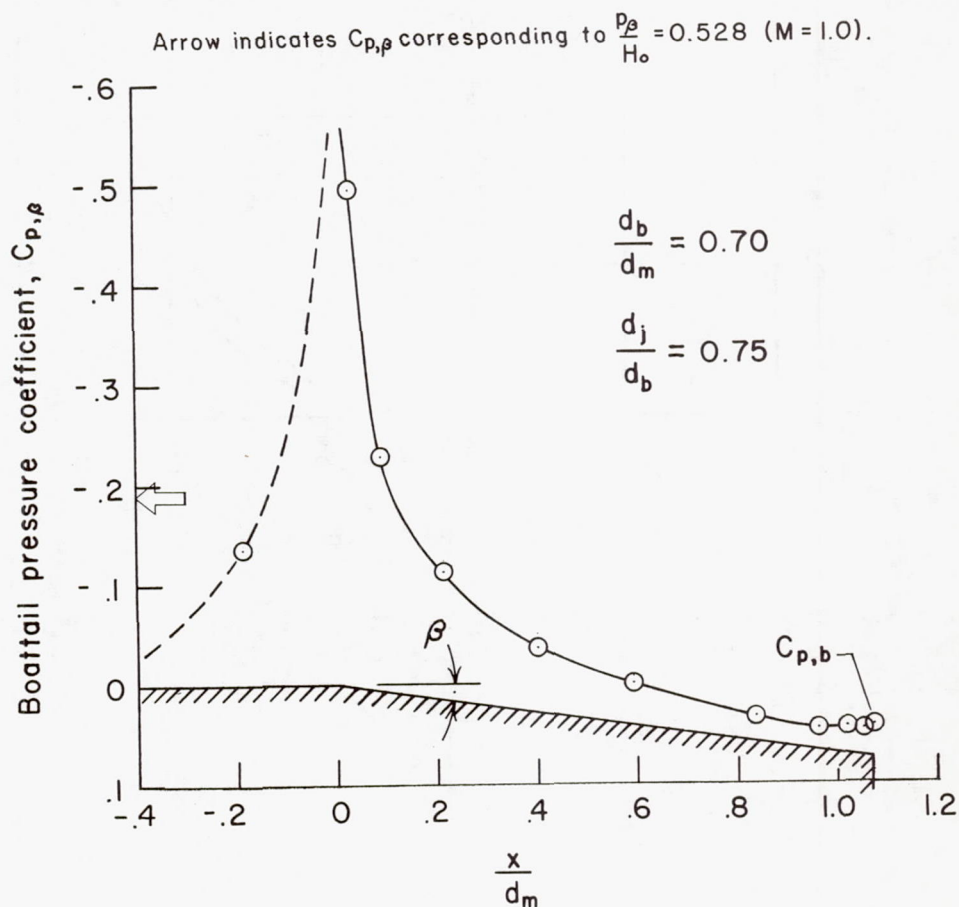
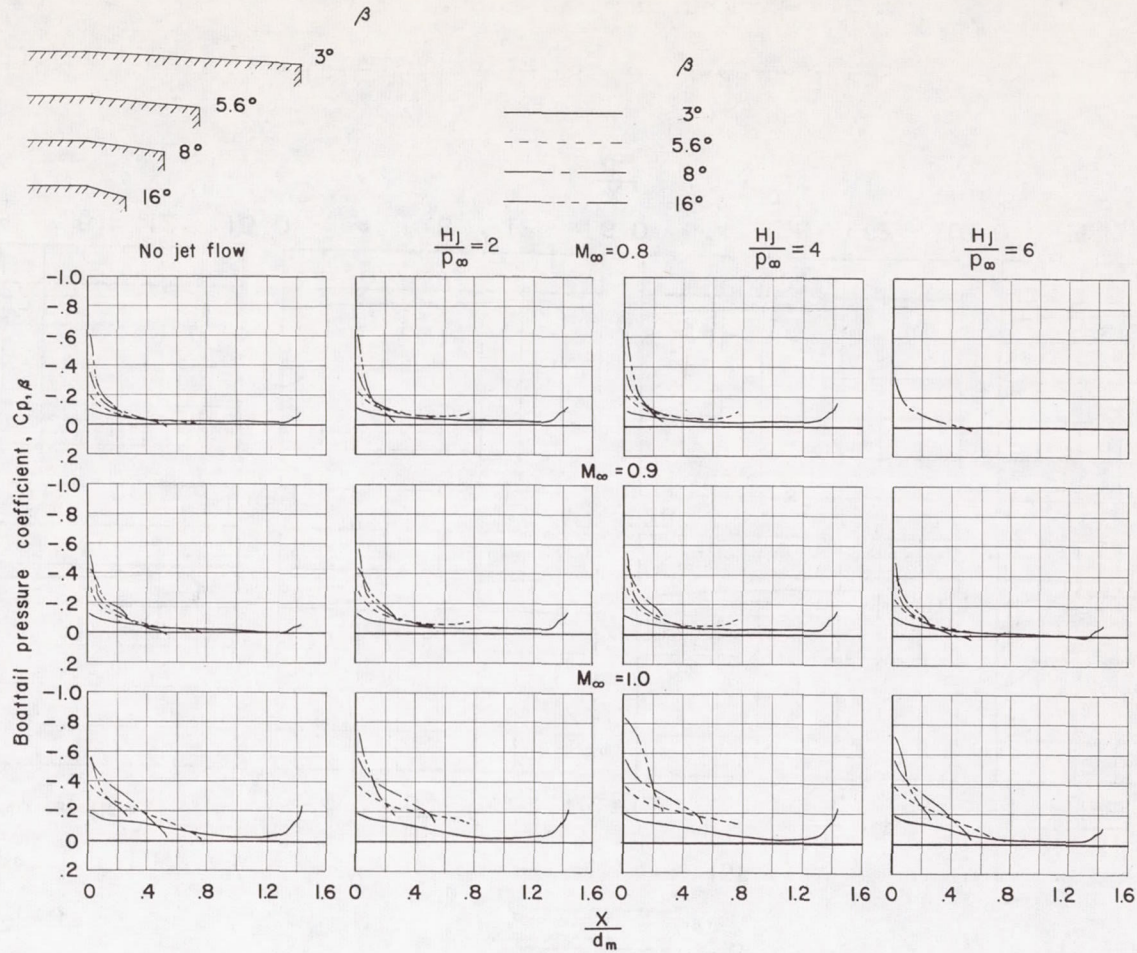
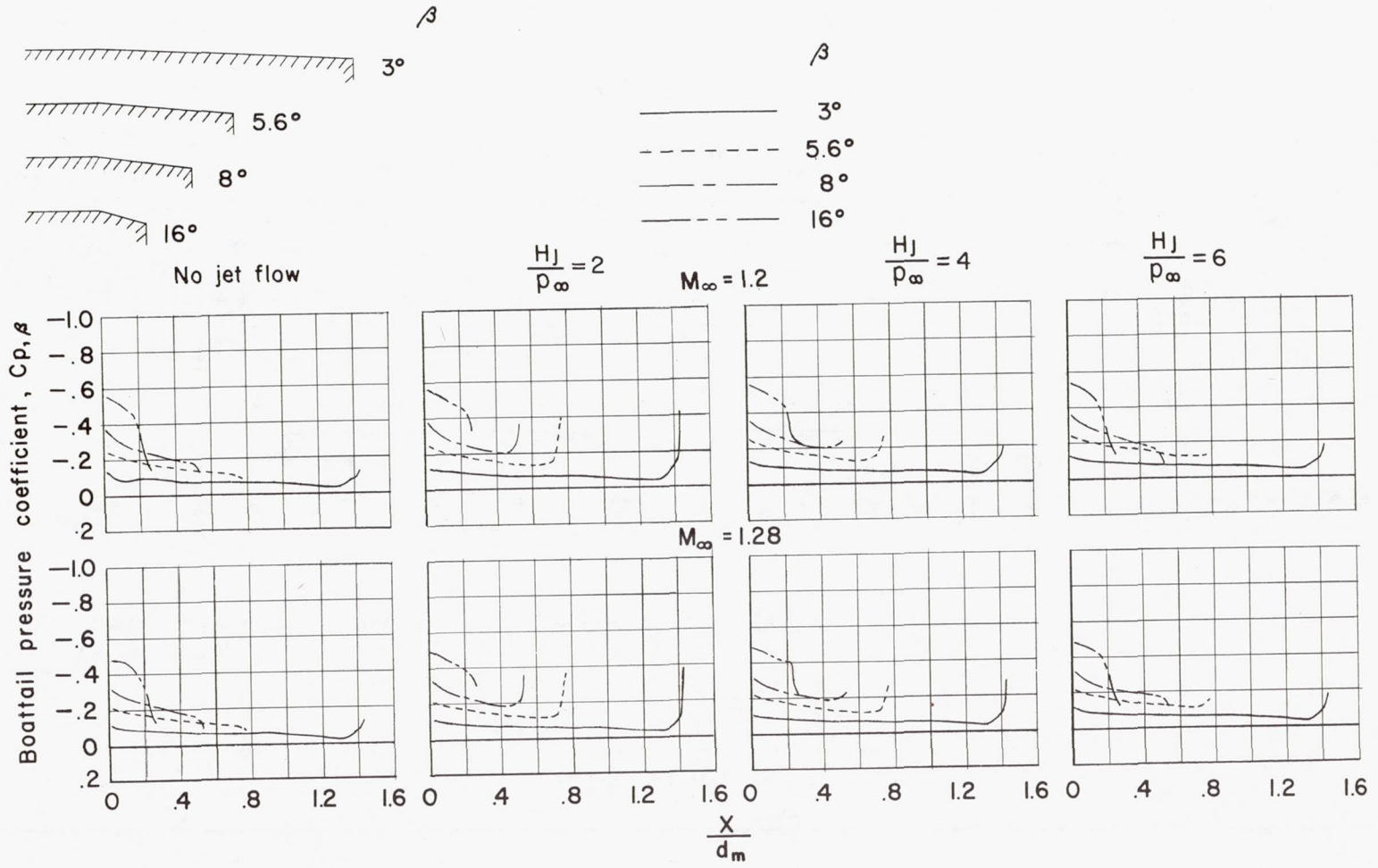


Figure 4.- Typical boattail pressure-coefficient distribution with jet flow. $M_\infty = 0.9$; $H_j/p_\infty = 4$.



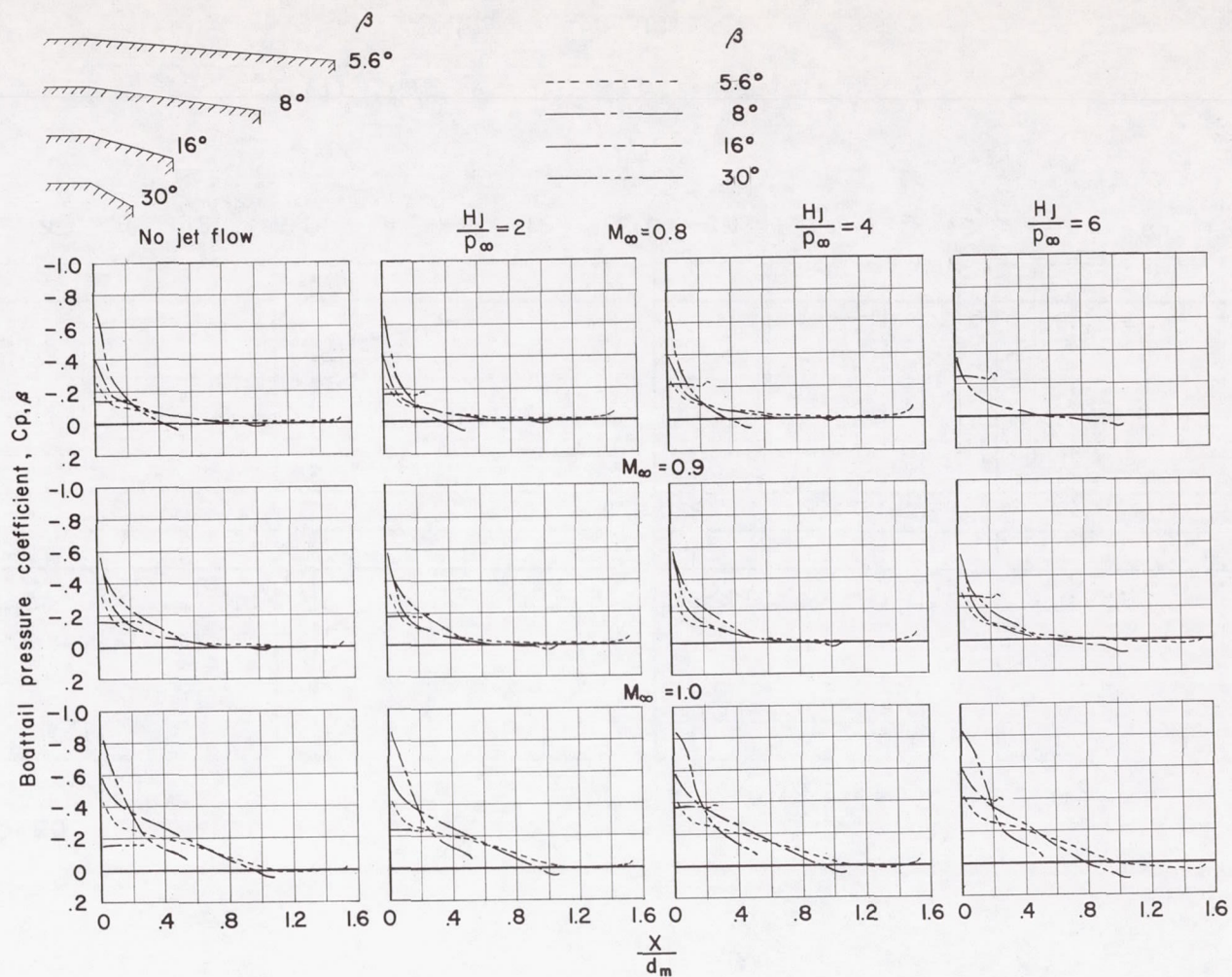
(a) $d_b/d_m = 0.85$; $M_\infty = 0.8, 0.9, \text{ and } 1.0$.

Figure 5.- Boattail pressure-coefficient distributions for several values of H_j/p_∞ and M_∞ .
 $d_j/d_b = 0.65$.



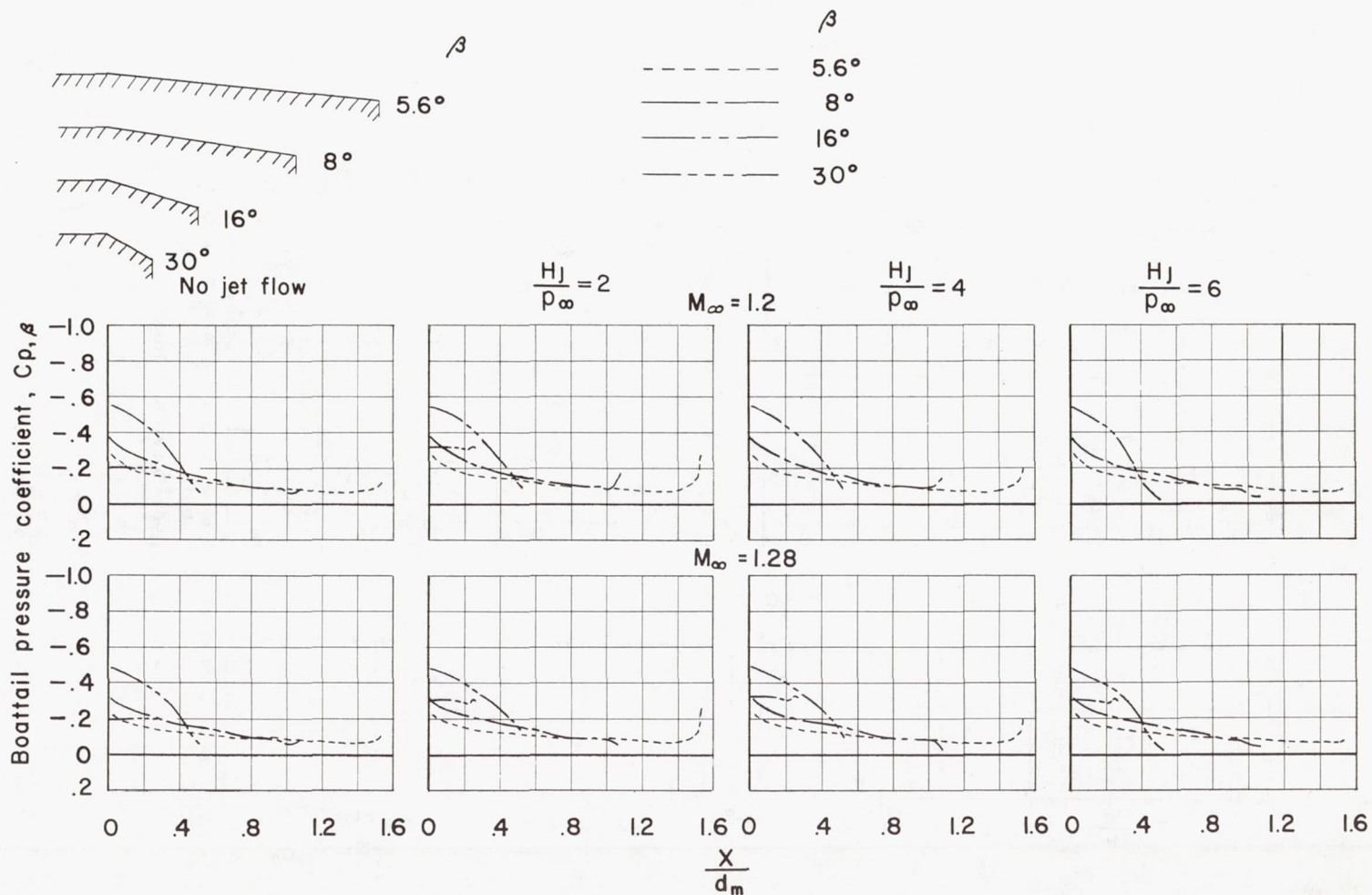
(b) $d_b/d_m = 0.85$; $M_\infty = 1.2$ and 1.28 .

Figure 5.- Continued.



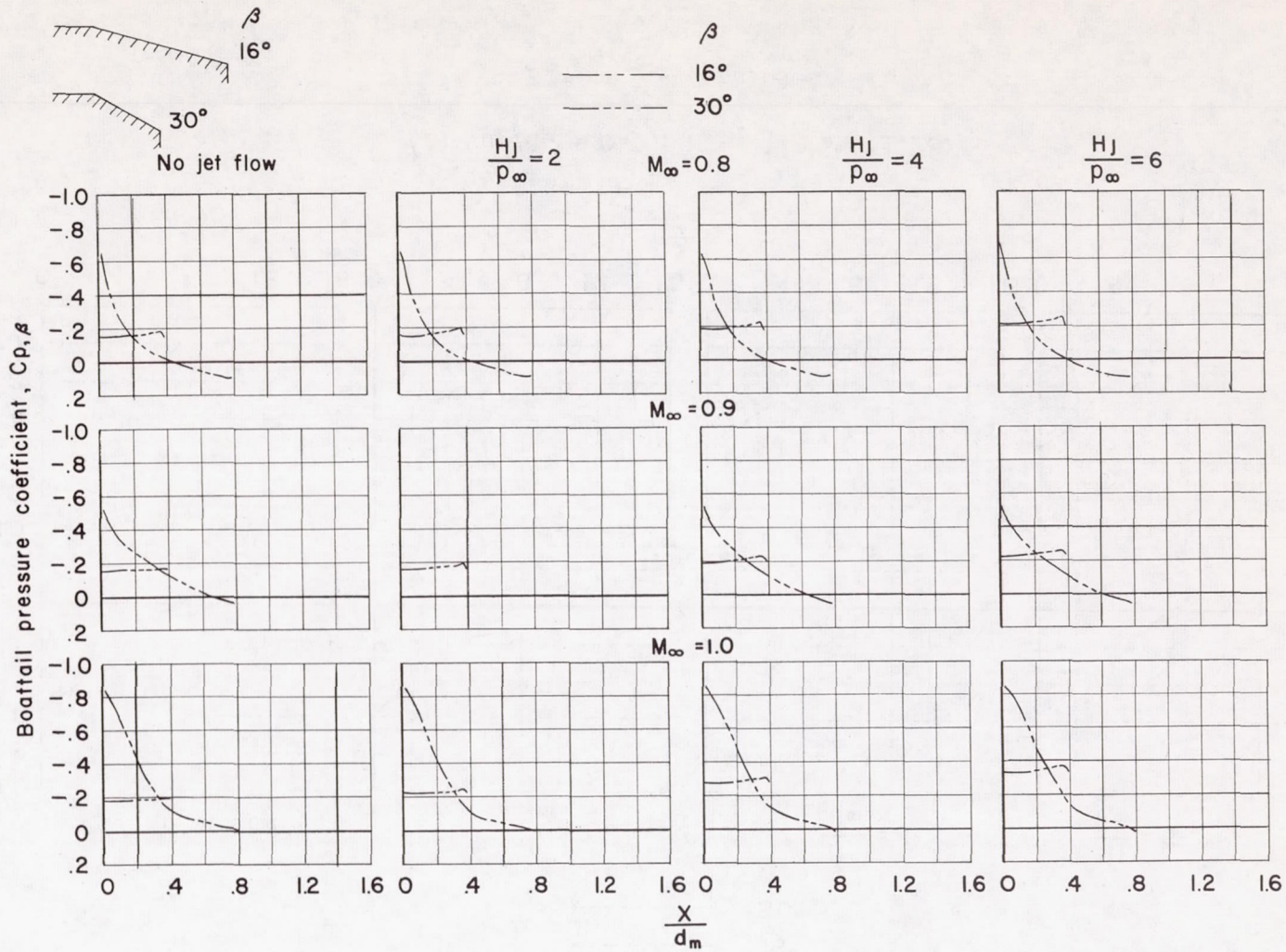
(c) $d_b/d_m = 0.70$; $M_\infty = 0.8, 0.9, \text{ and } 1.0$.

Figure 5.- Continued.



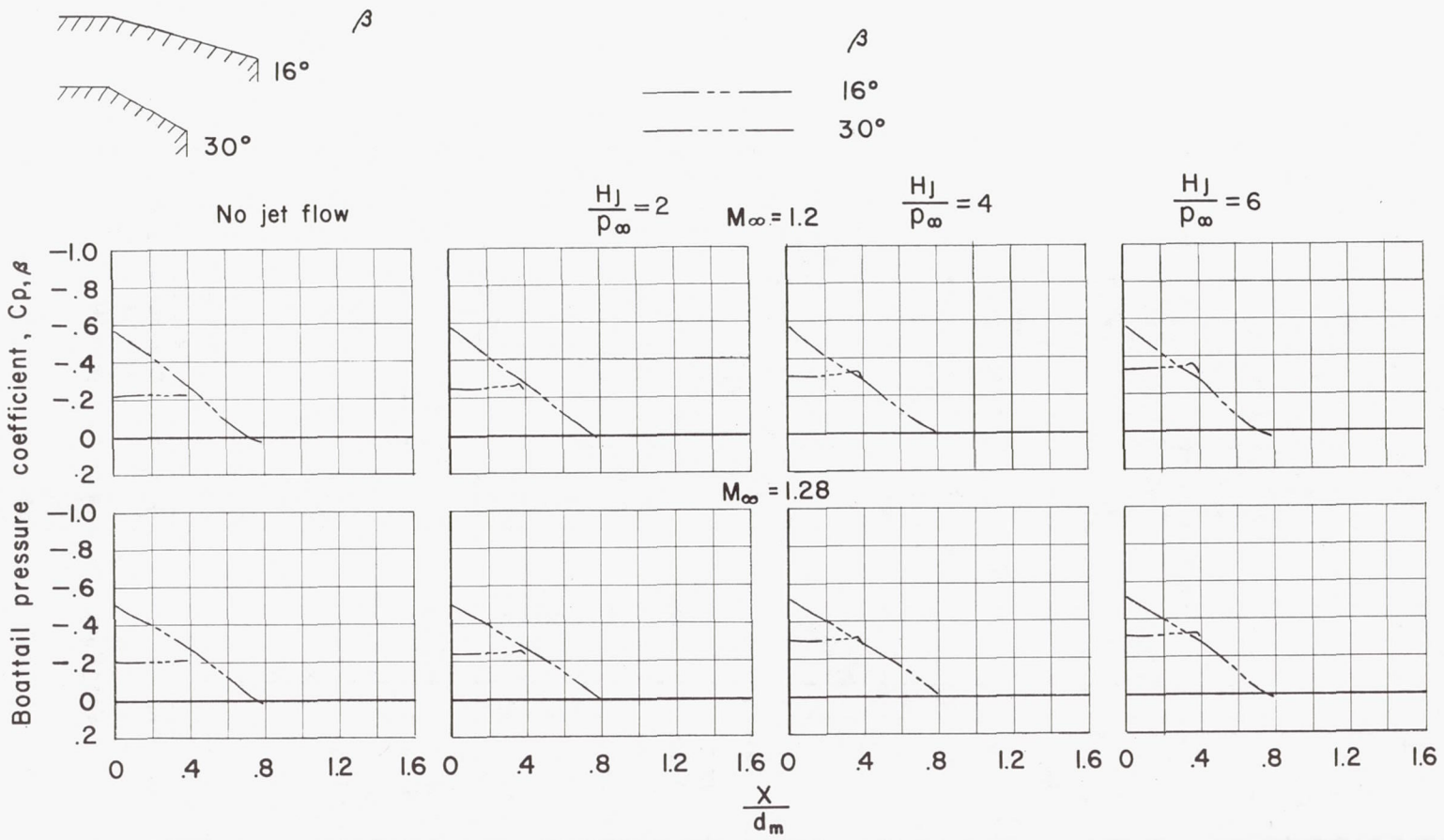
(d) $d_b/d_m = 0.70$; $M_\infty = 1.2$ and 1.28 .

Figure 5.- Continued.



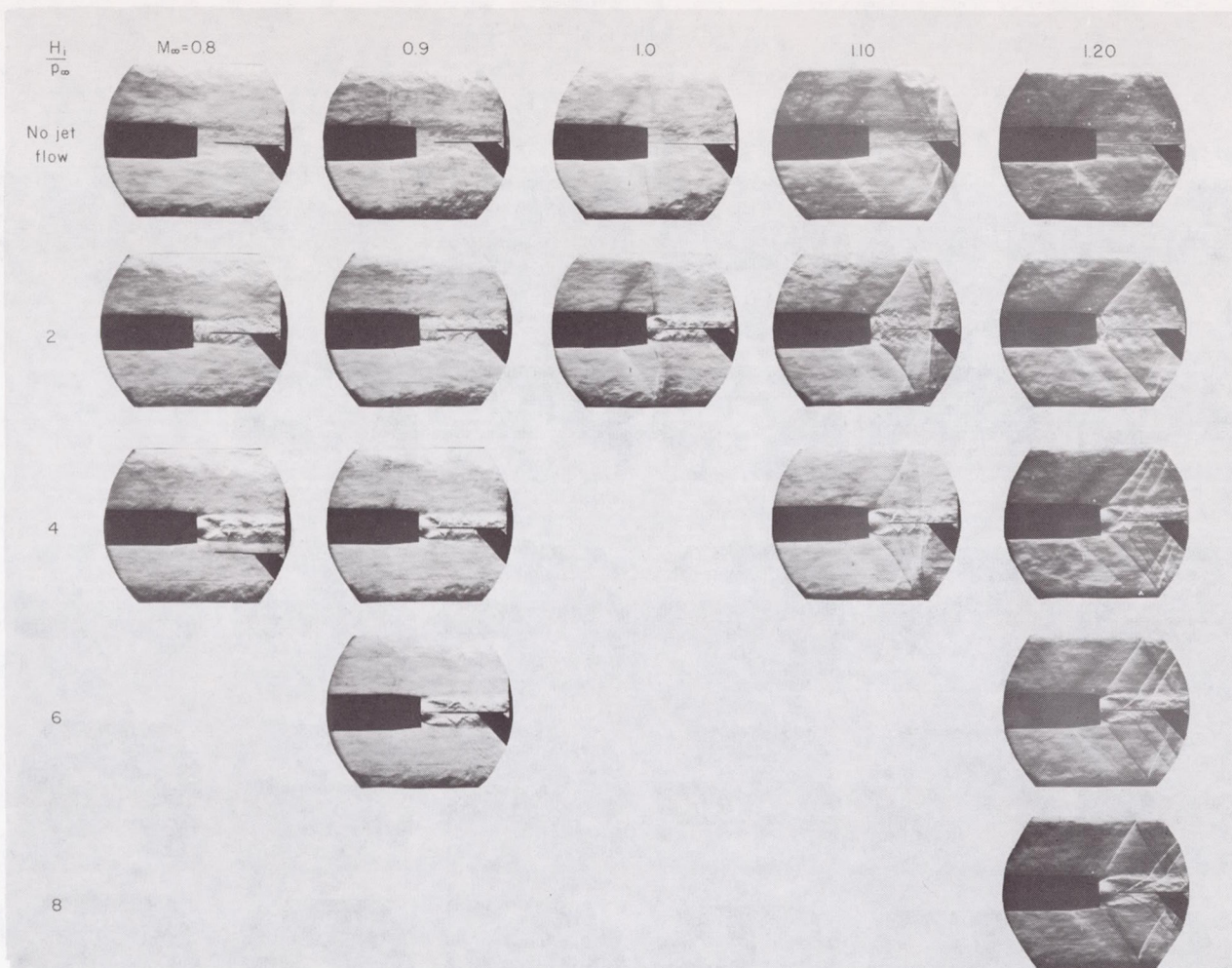
(e) $d_b/d_m = 0.55$; $M_\infty = 0.8, 0.9, \text{ and } 1.0$.

Figure 5.- Continued.



(f) $d_b/d_m = 0.55$; $M_\infty = 1.2$ and 1.28 .

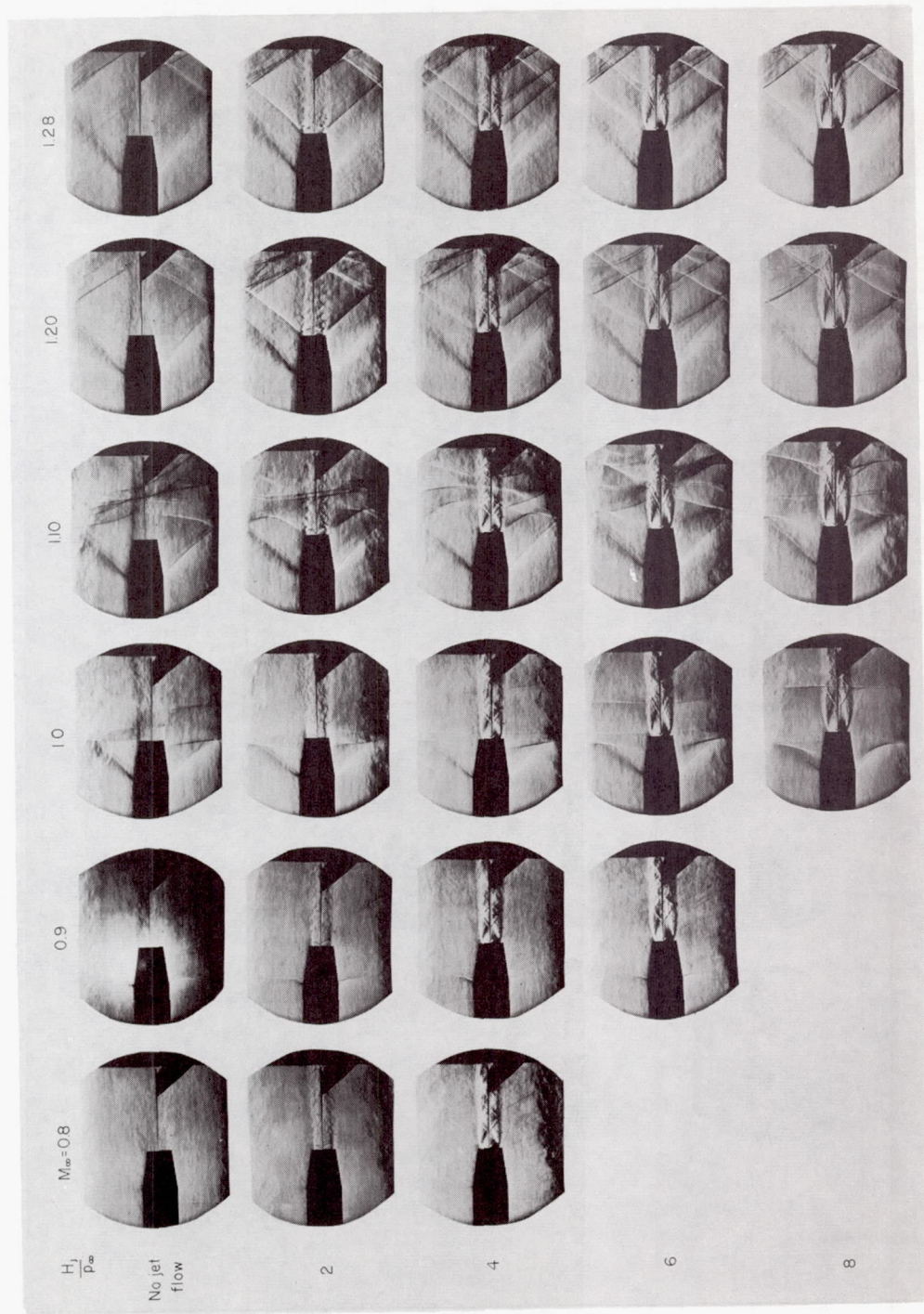
Figure 5.- Concluded.



(a) $\beta = 5.6^\circ$; $d_b/d_m = 0.85$; $d_j/d_b = 0.65$.

L-57-168

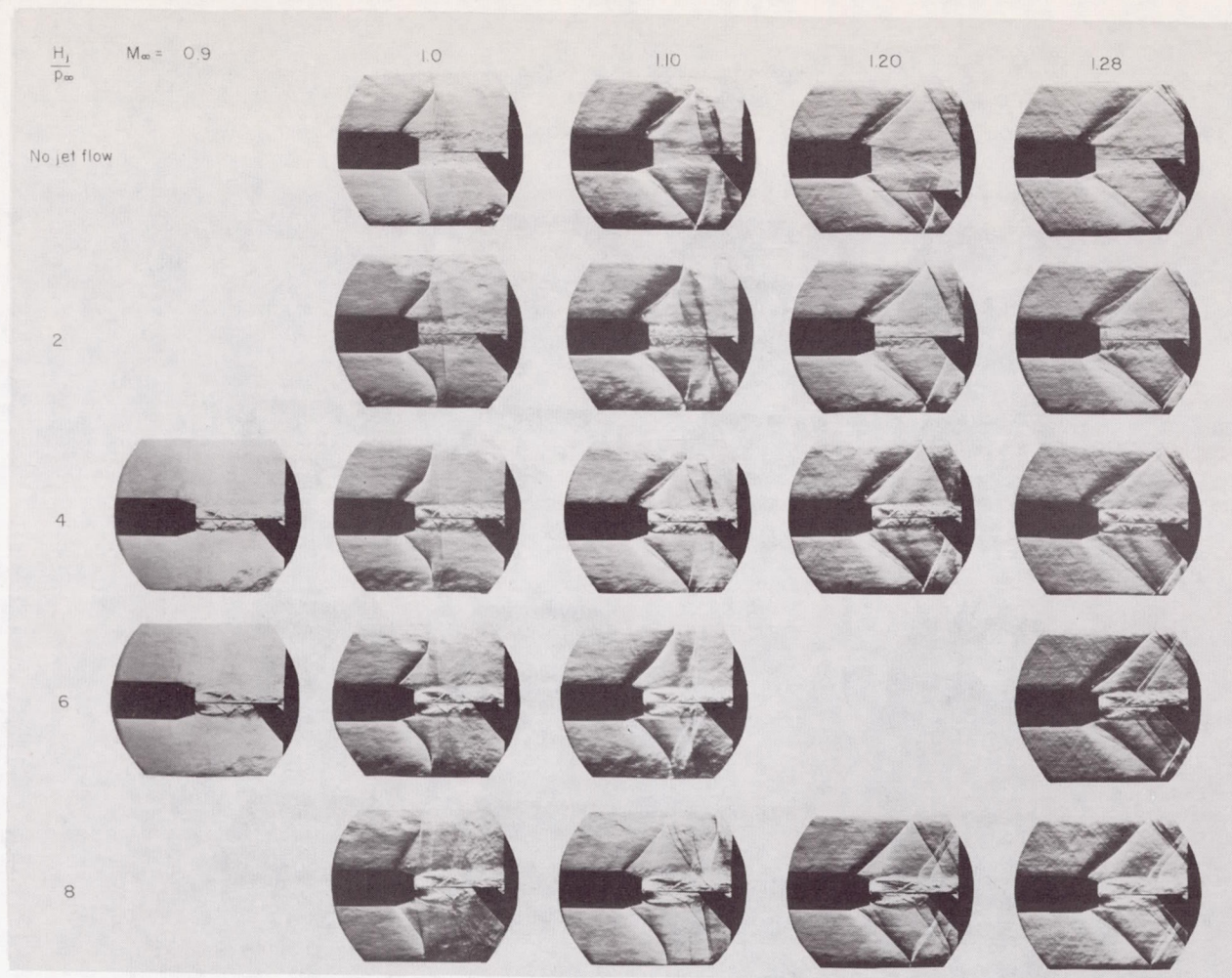
Figure 6.- Schlieren photographs of flow about several afterbody configurations.



L-57-169

(b) $\beta = 8^\circ$; $d_b/d_m = 0.70$; $d_j/d_b = 0.75$.

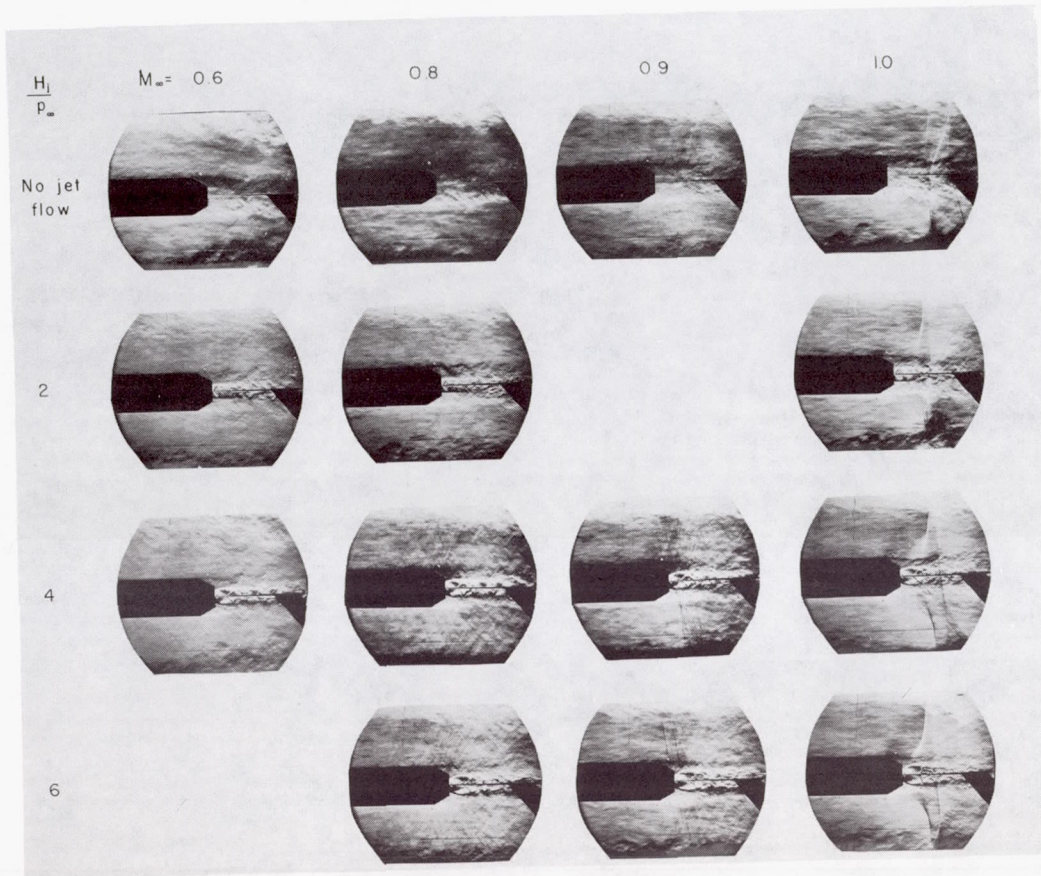
Figure 6.- Continued.



(c) $\beta = 16^\circ$; $d_b/d_m = 0.70$; $d_j/d_b = 0.75$.

L-57-170

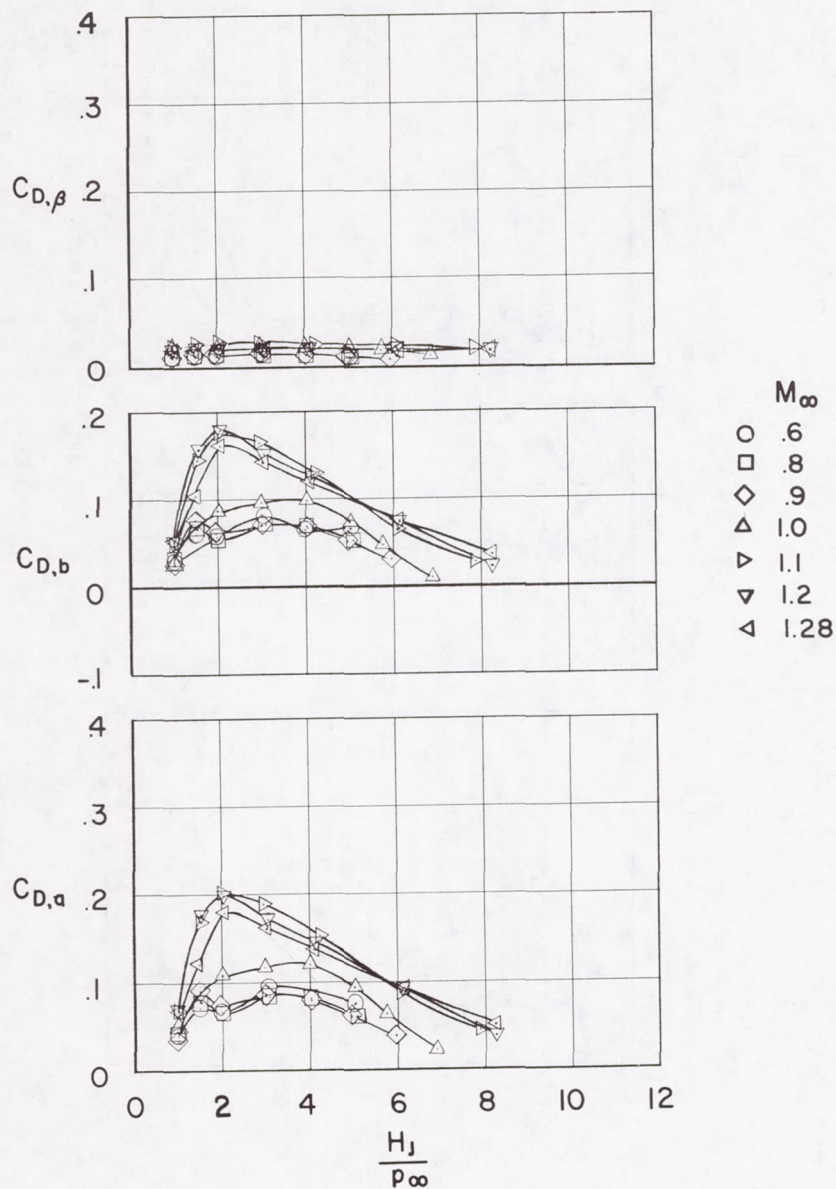
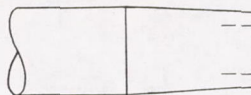
Figure 6.- Continued.



(d) $\beta = 30^\circ$; $d_b/d_m = 0.55$; $d_j/d_b = 0.75$.

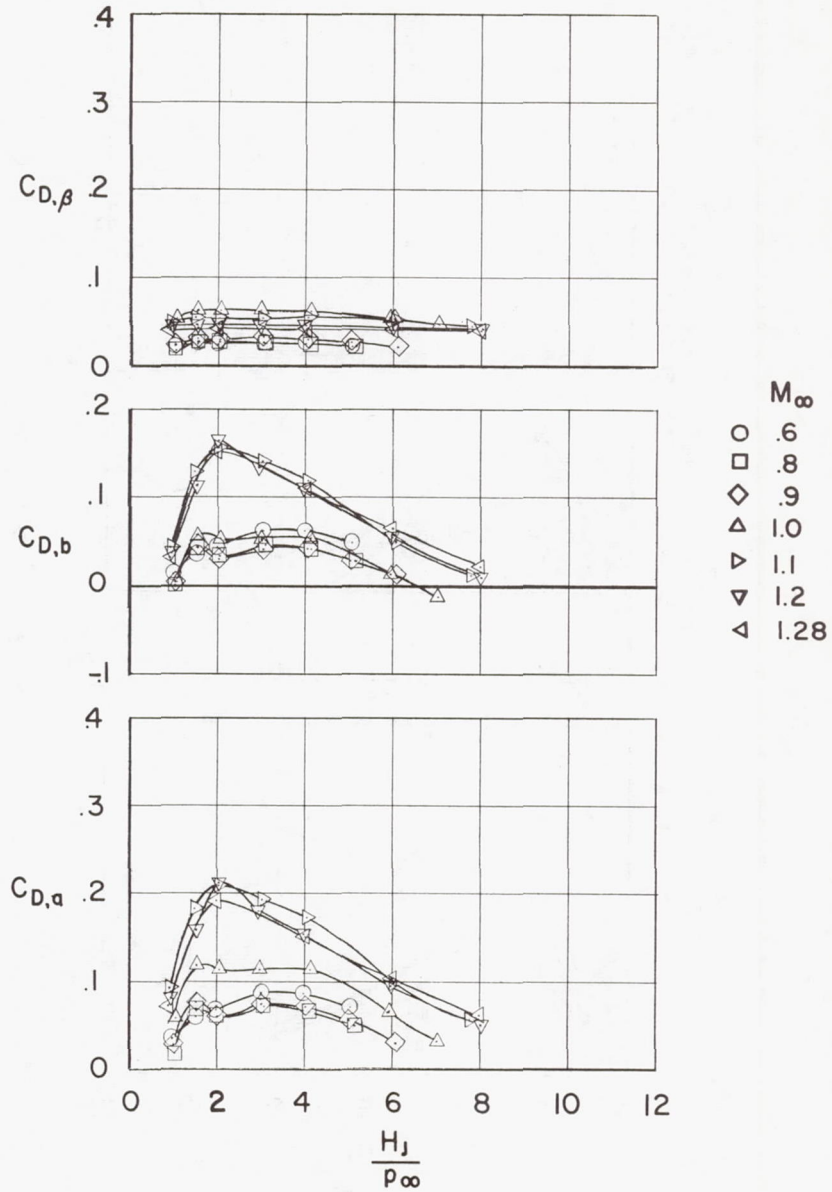
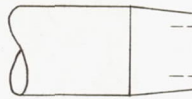
L-57-171

Figure 6.- Concluded.



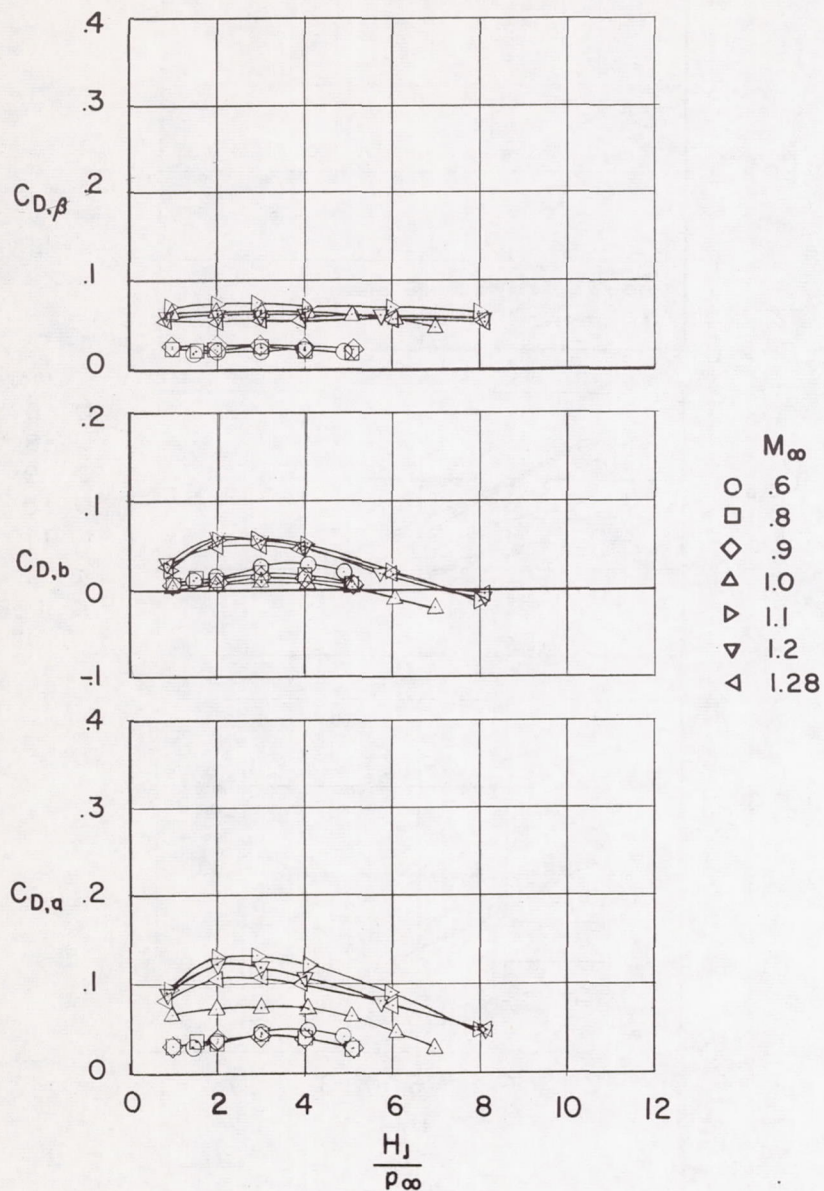
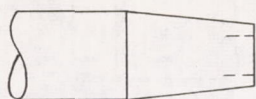
(a) $\beta = 3^\circ$; $d_b/d_m = 0.85$.

Figure 7.- Variation of boattail, base, and afterbody drag coefficient with jet total pressure at constant values of M_∞ . $d_j/d_b = 0.65$.



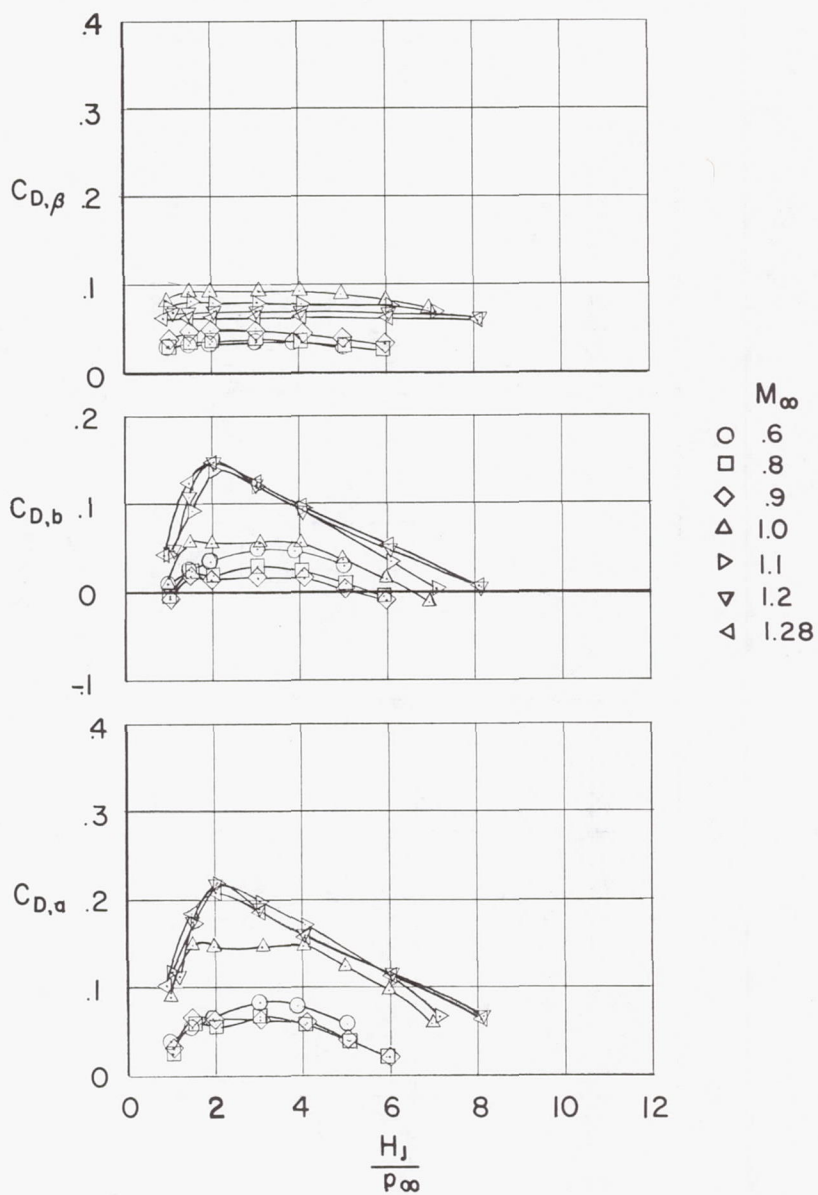
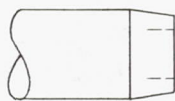
(b) $\beta = 5.6^\circ$; $d_b/d_m = 0.85$.

Figure 7.- Continued.



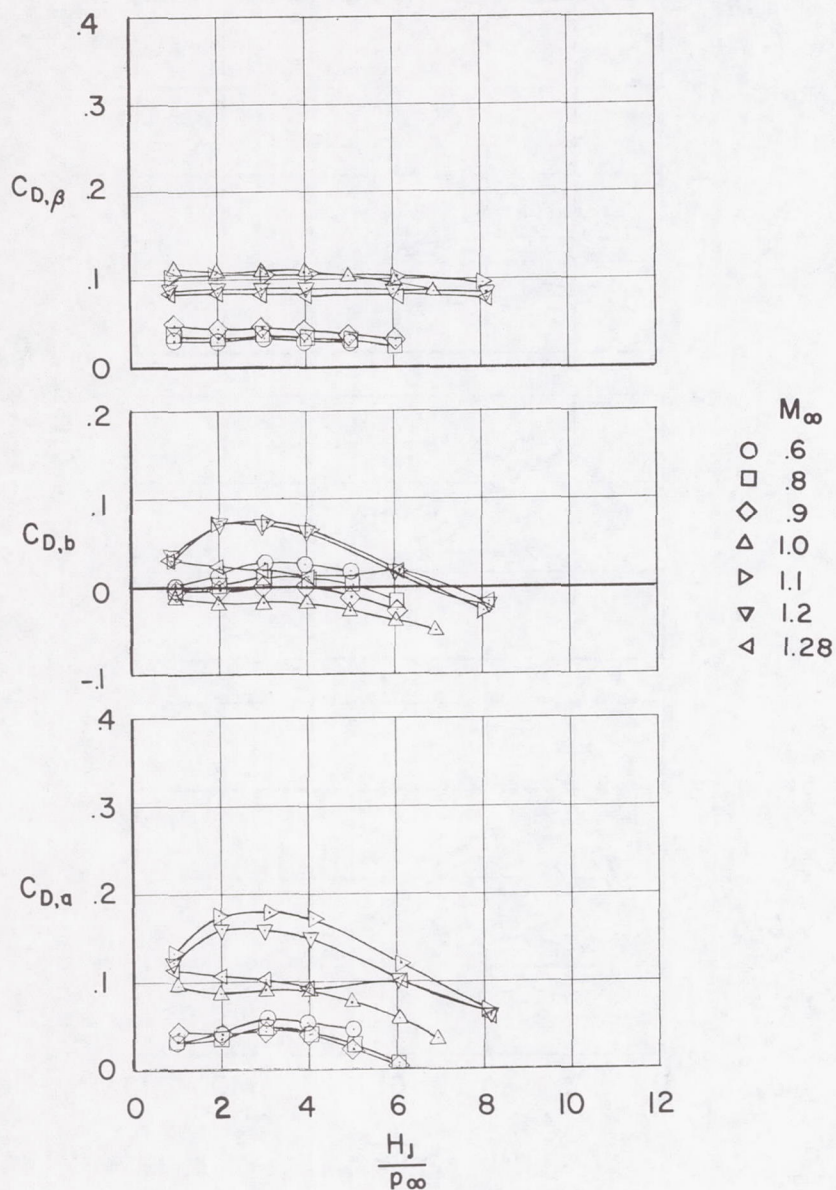
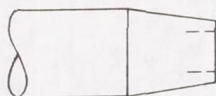
(c) $\beta = 5.6^\circ$; $d_b/d_m = 0.70$.

Figure 7.- Continued.



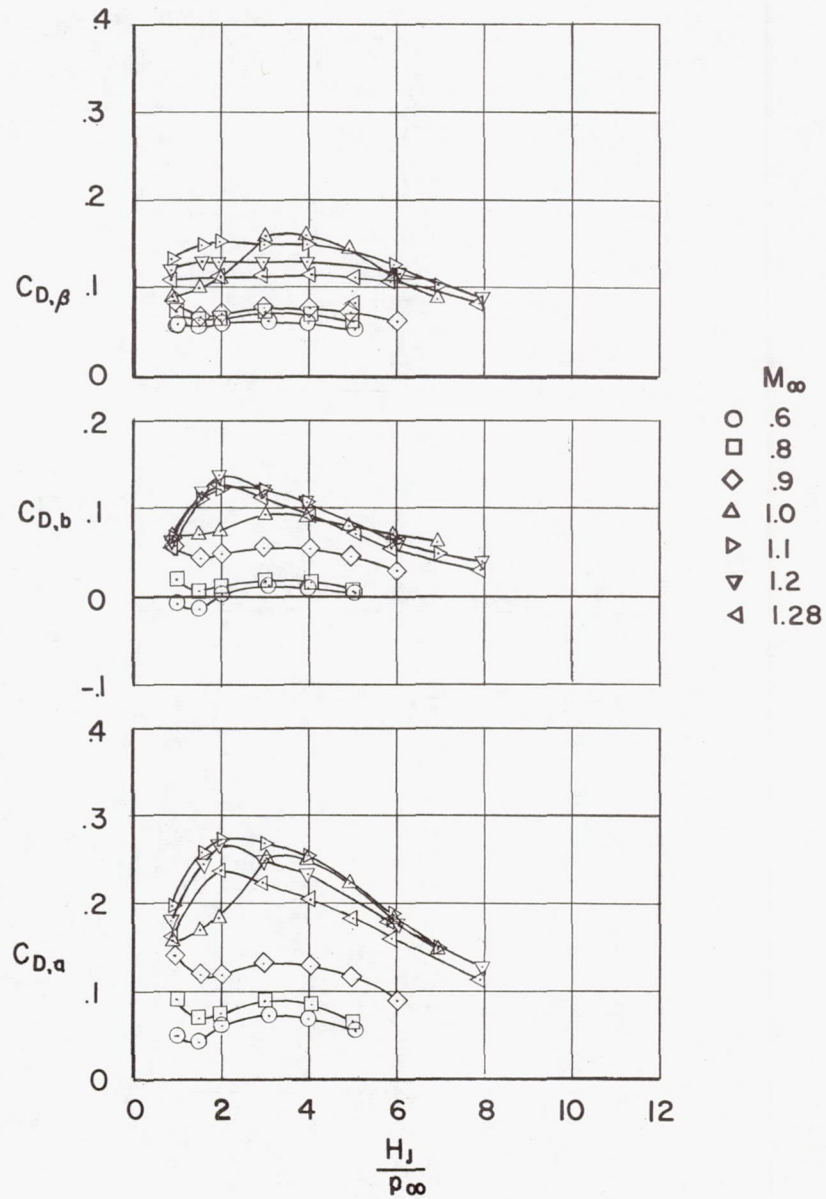
(d) $\beta = 8^\circ$; $d_b/d_m = 0.85$.

Figure 7.- Continued.



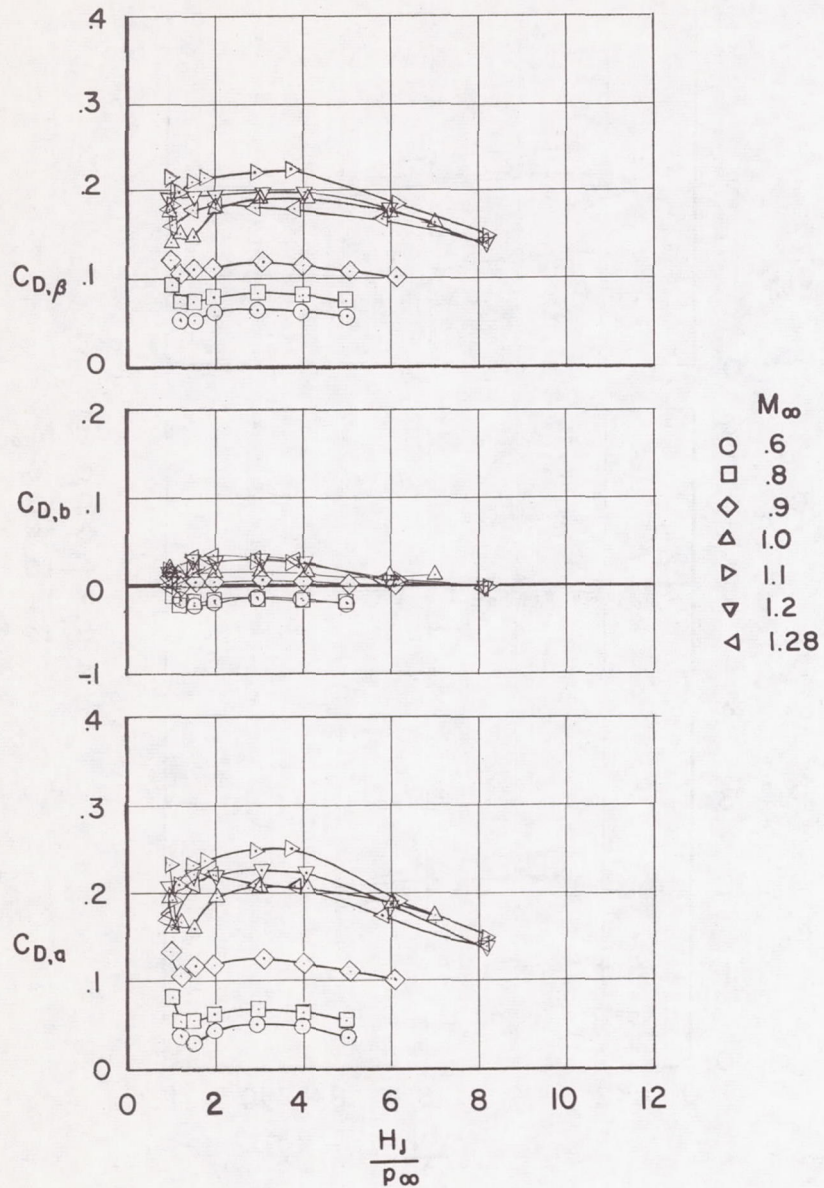
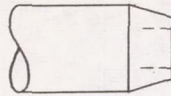
(e) $\beta = 8^\circ$; $d_b/d_m = 0.70$.

Figure 7.- Continued.



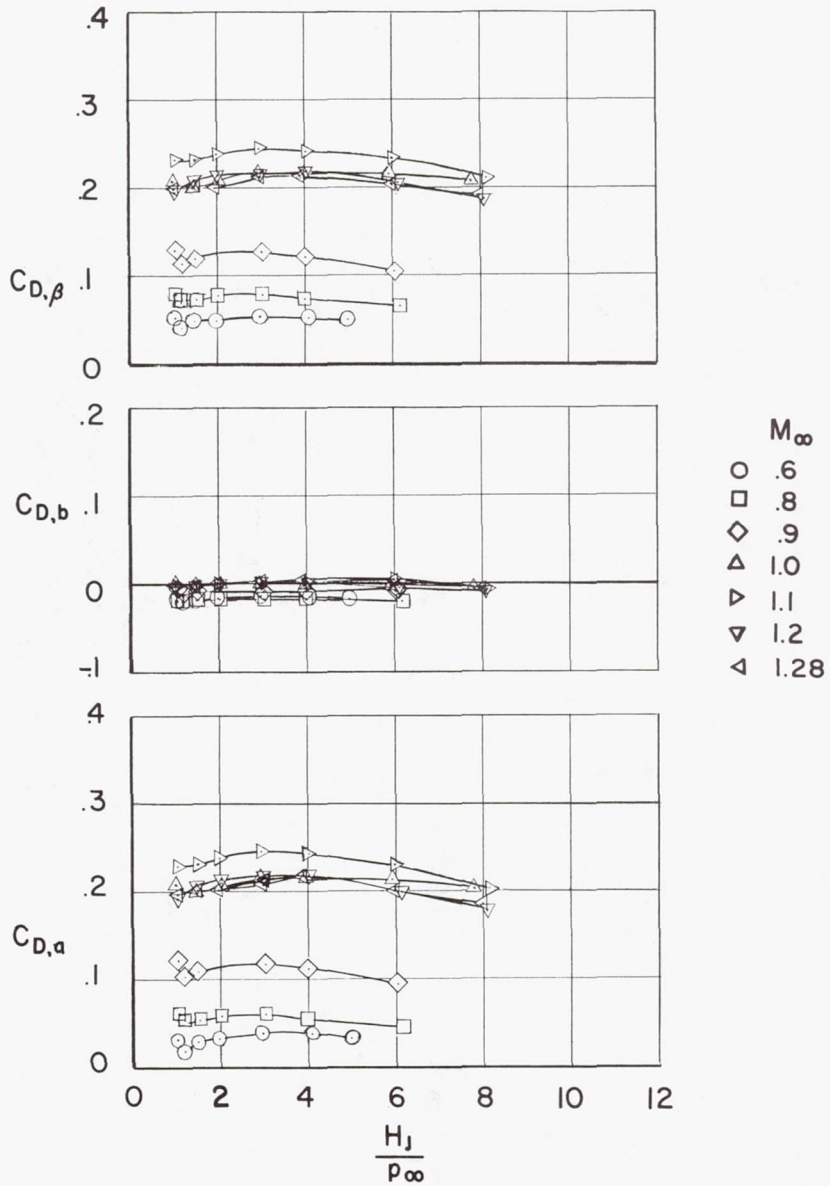
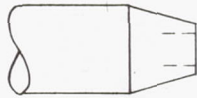
(f) $\beta = 16^\circ$; $d_b/d_m = 0.85$.

Figure 7.- Continued.



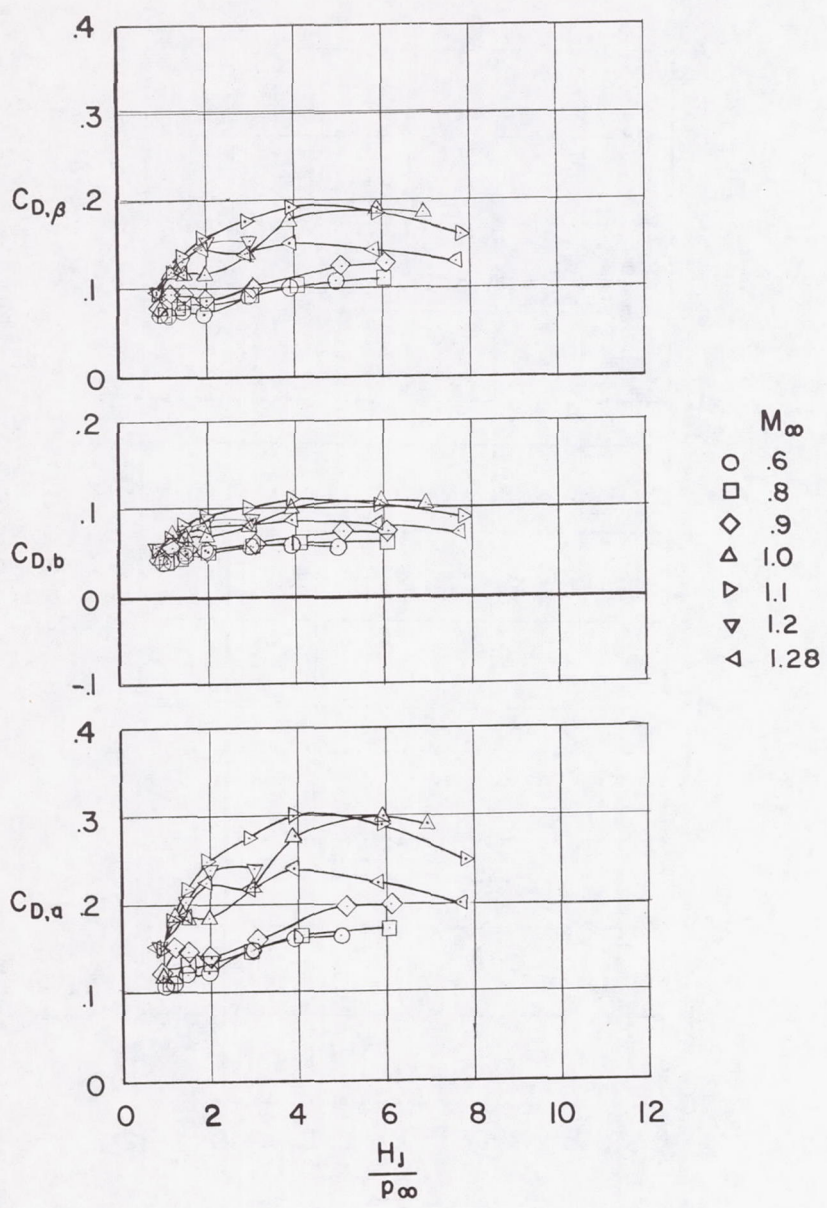
(g) $\beta = 16^\circ$; $d_b/d_m = 0.70$.

Figure 7.- Continued.



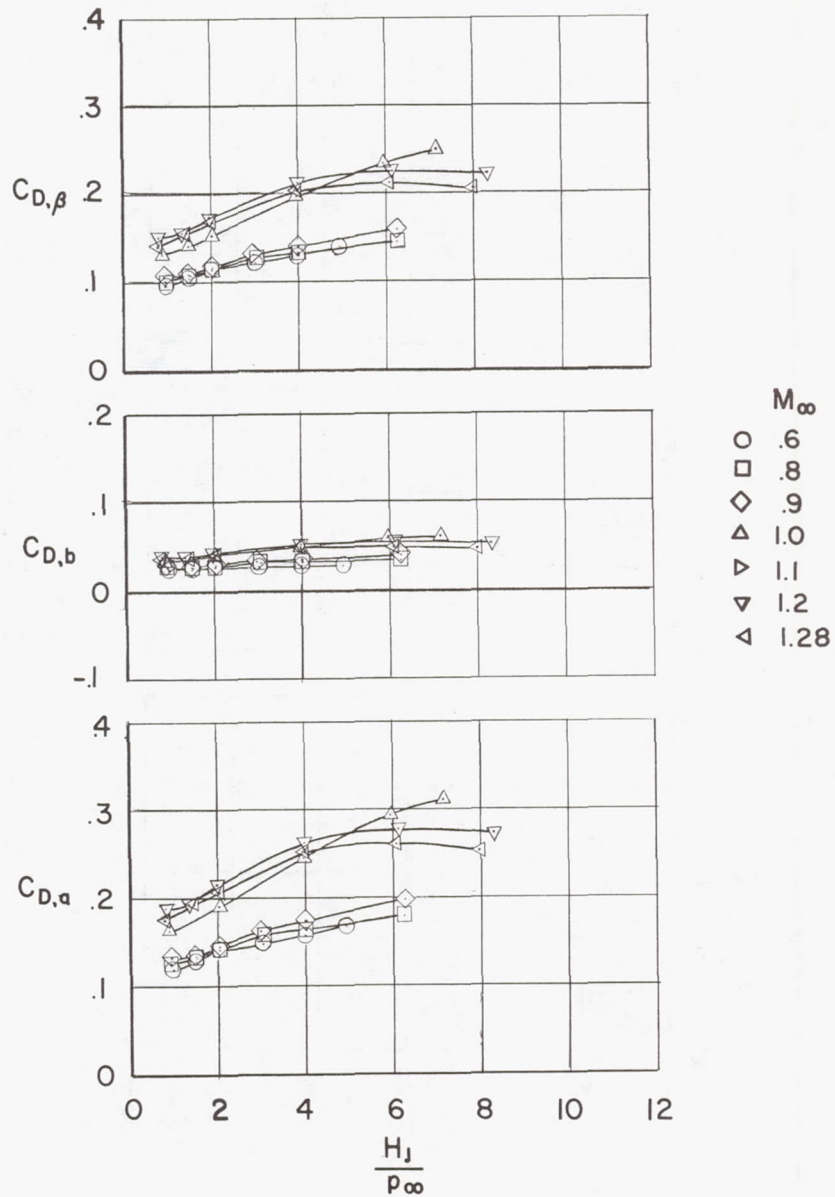
(h) $\beta = 16^\circ$; $d_b/d_m = 0.55$.

Figure 7.- Continued.



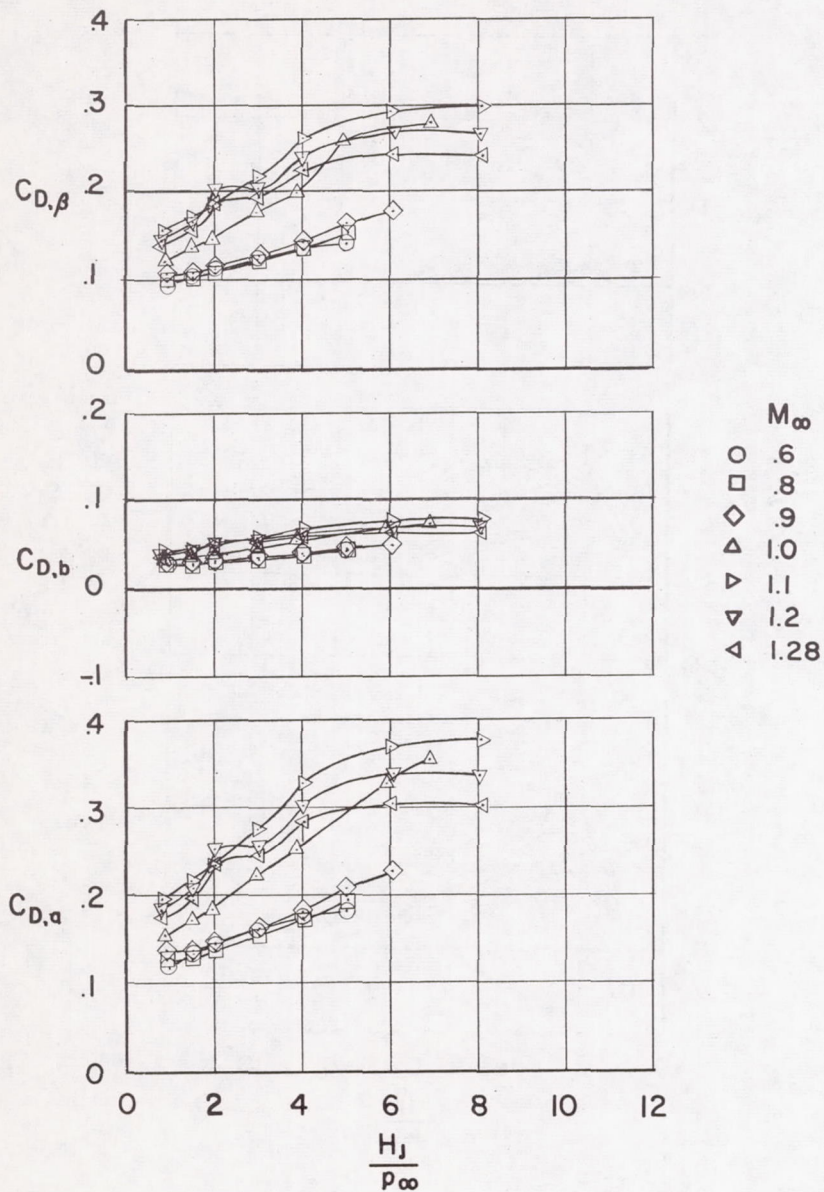
(i) $\beta = 30^\circ$; $d_b/d_m = 0.70$.

Figure 7.- Continued.



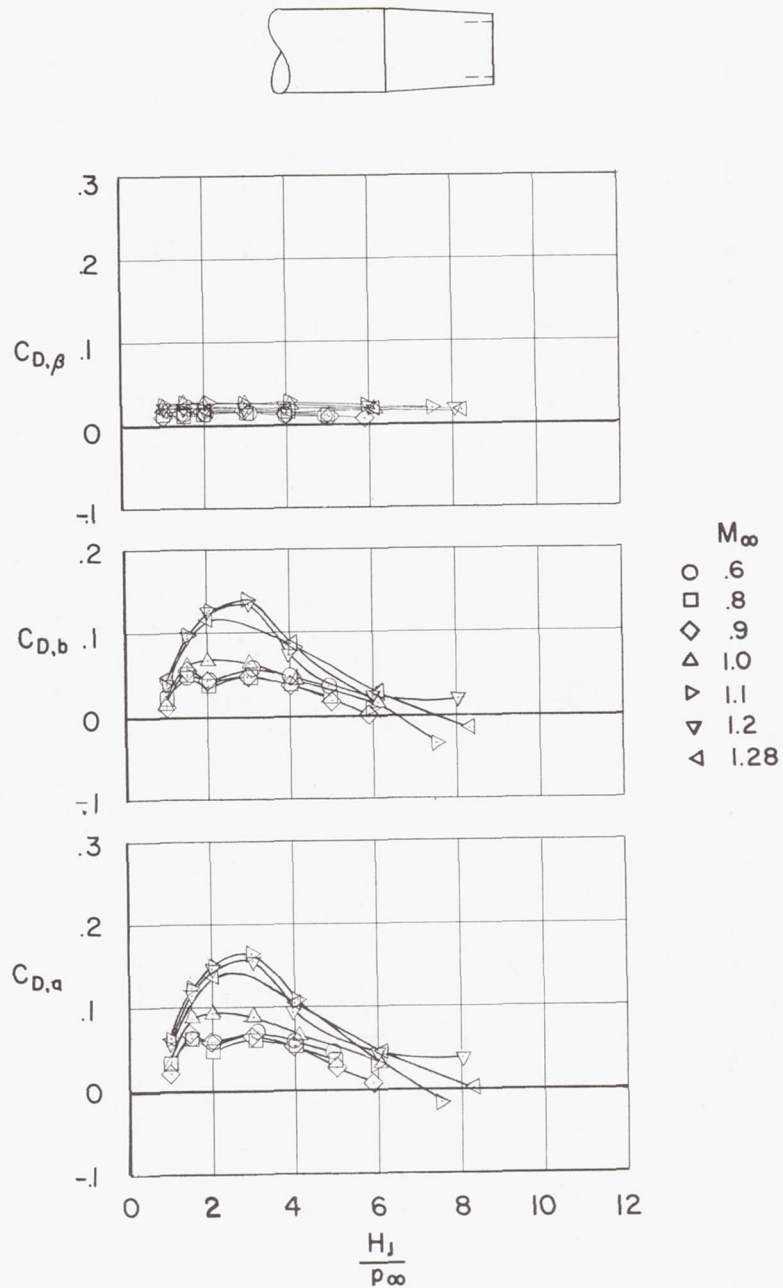
(j) $\beta = 30^\circ$; $d_b/d_m = 0.55$.

Figure 7.- Continued.



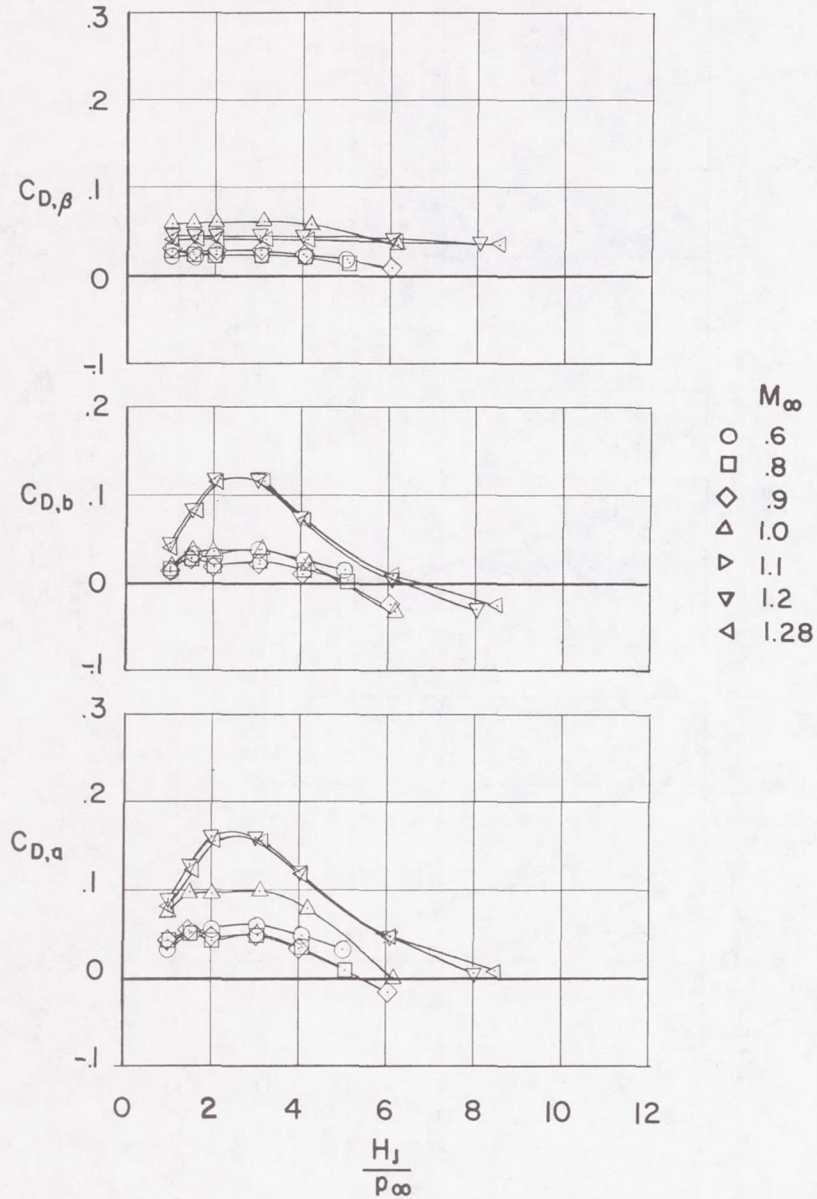
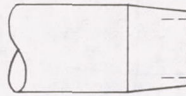
(k) $\beta = 45^\circ$; $d_b/d_m = 0.55$.

Figure 7.- Concluded.



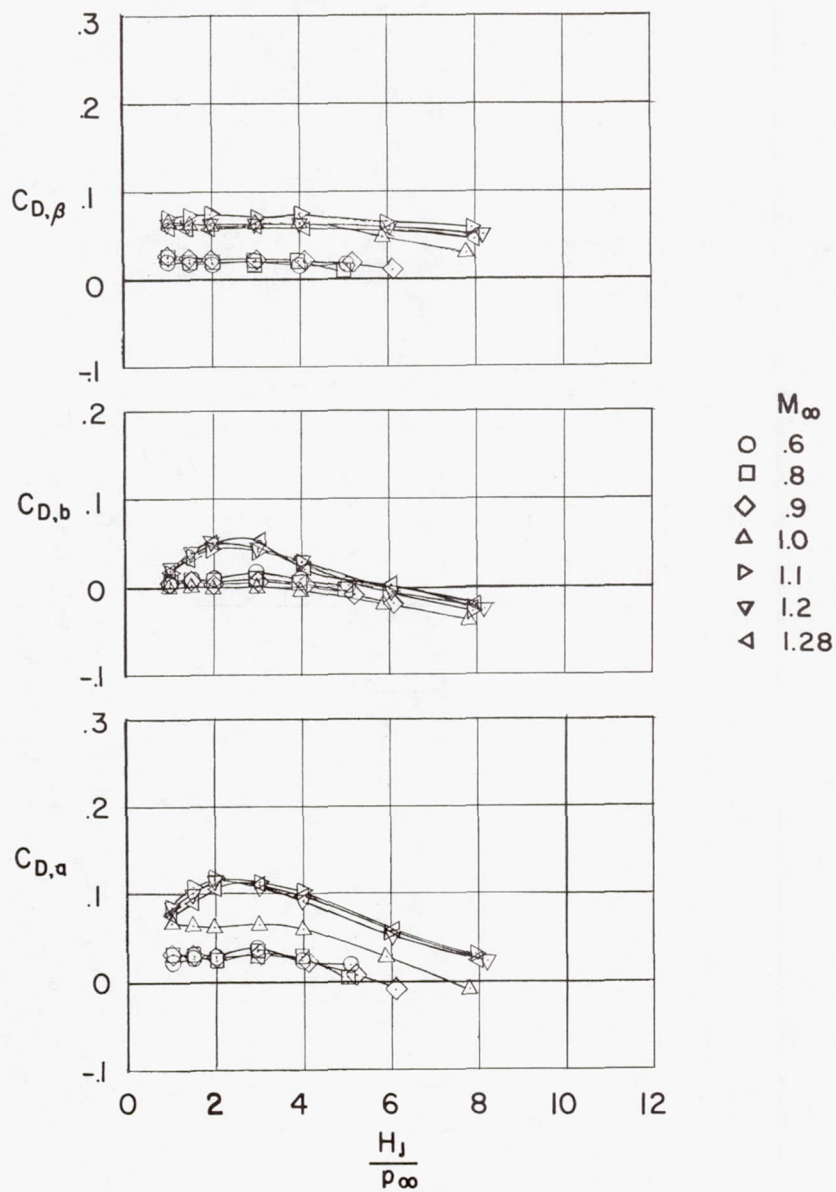
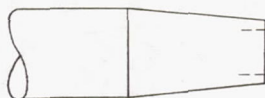
(a) $\beta = 3^\circ$; $d_b/d_m = 0.85$.

Figure 8.- Variation of boattail, base, and afterbody drag coefficient with jet total-pressure ratio at constant values of M_∞ . $d_j/d_b = 0.75$.



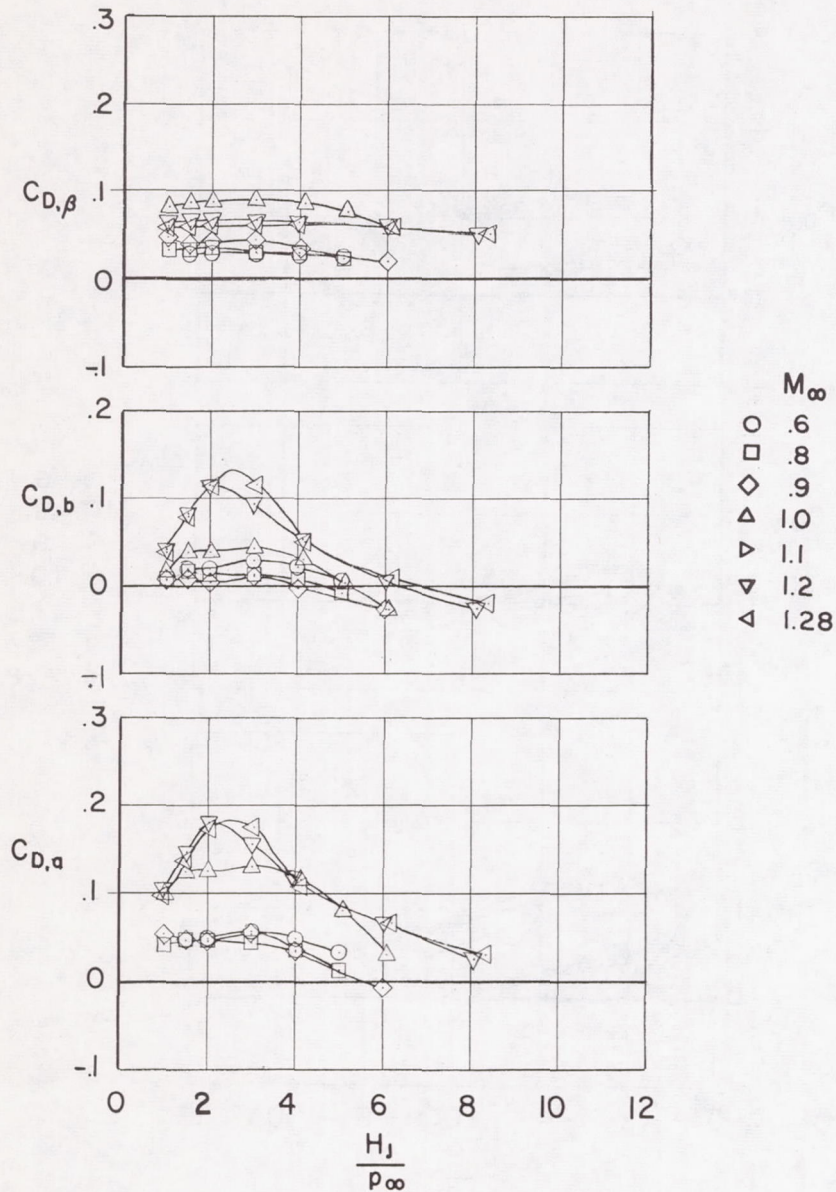
(b) $\beta = 5.6^\circ$; $d_b/d_m = 0.85$.

Figure 8.- Continued.



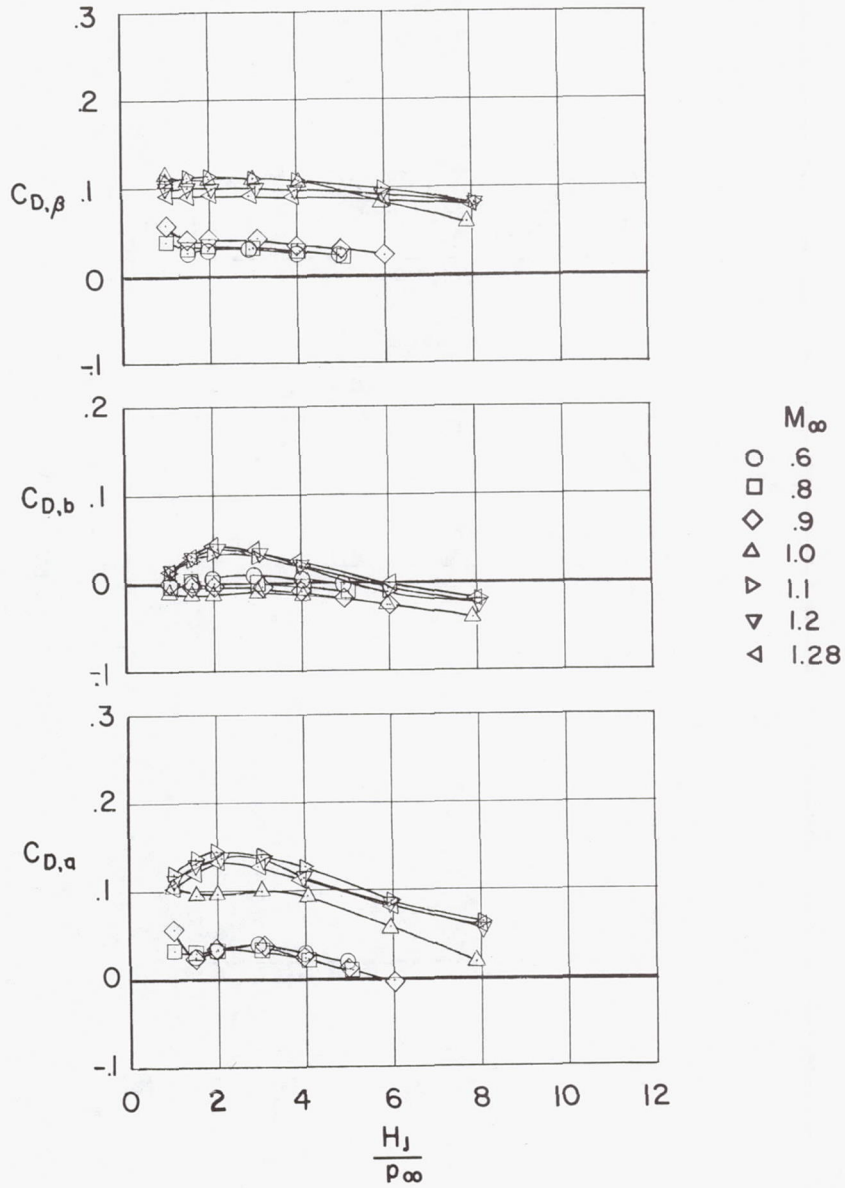
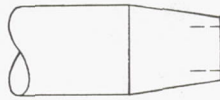
(c) $\beta = 5.6^\circ$; $d_b/d_m = 0.70$.

Figure 8.- Continued.



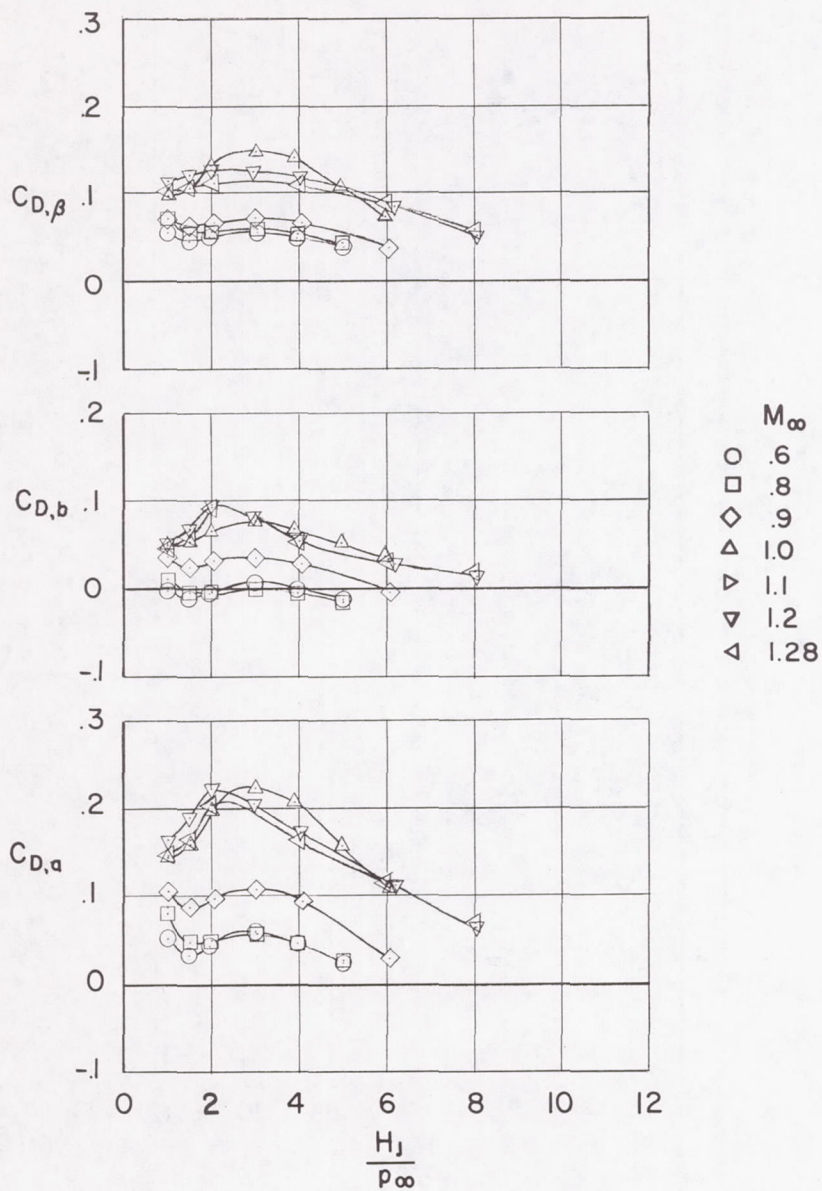
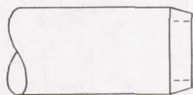
(d) $\beta = 8^\circ$; $d_b/d_m = 0.85$.

Figure 8.- Continued.



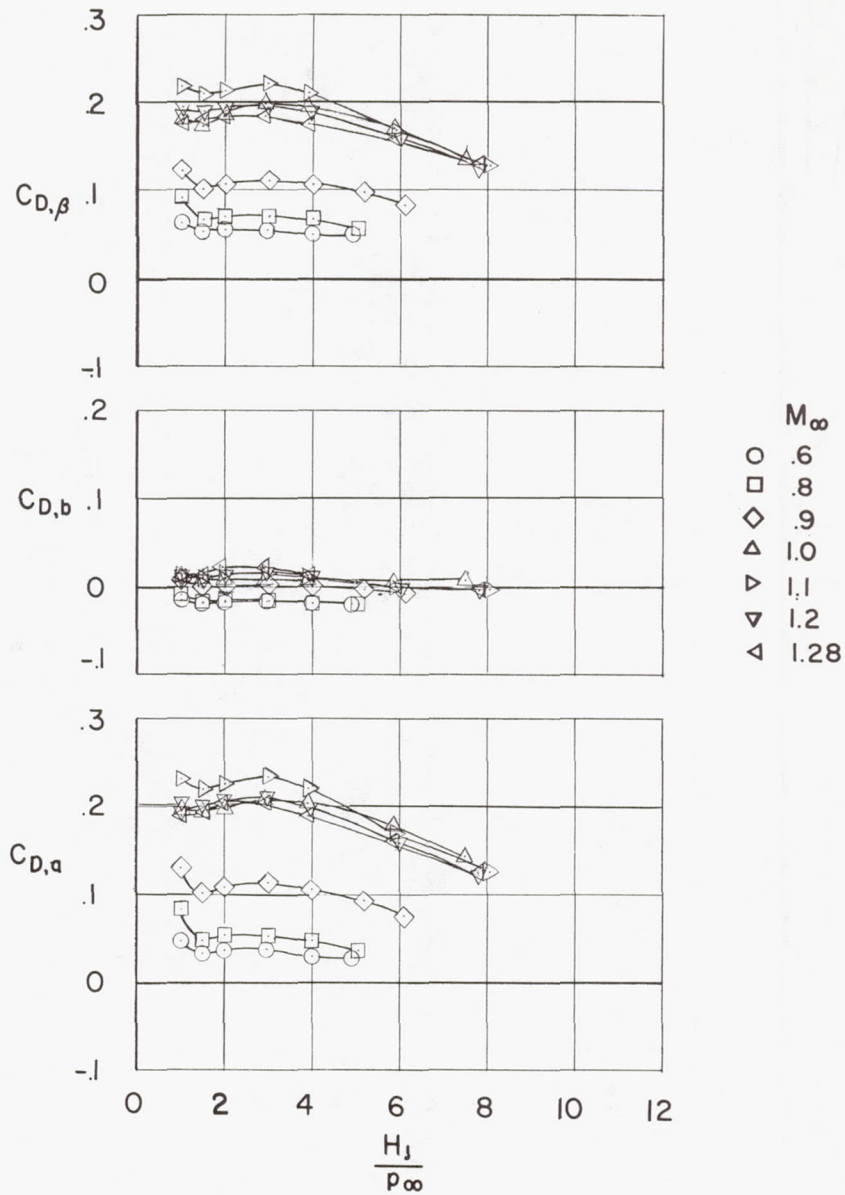
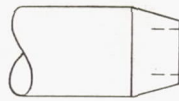
(e) $\beta = 8^\circ$; $d_b/d_m = 0.70$.

Figure 8.- Continued.



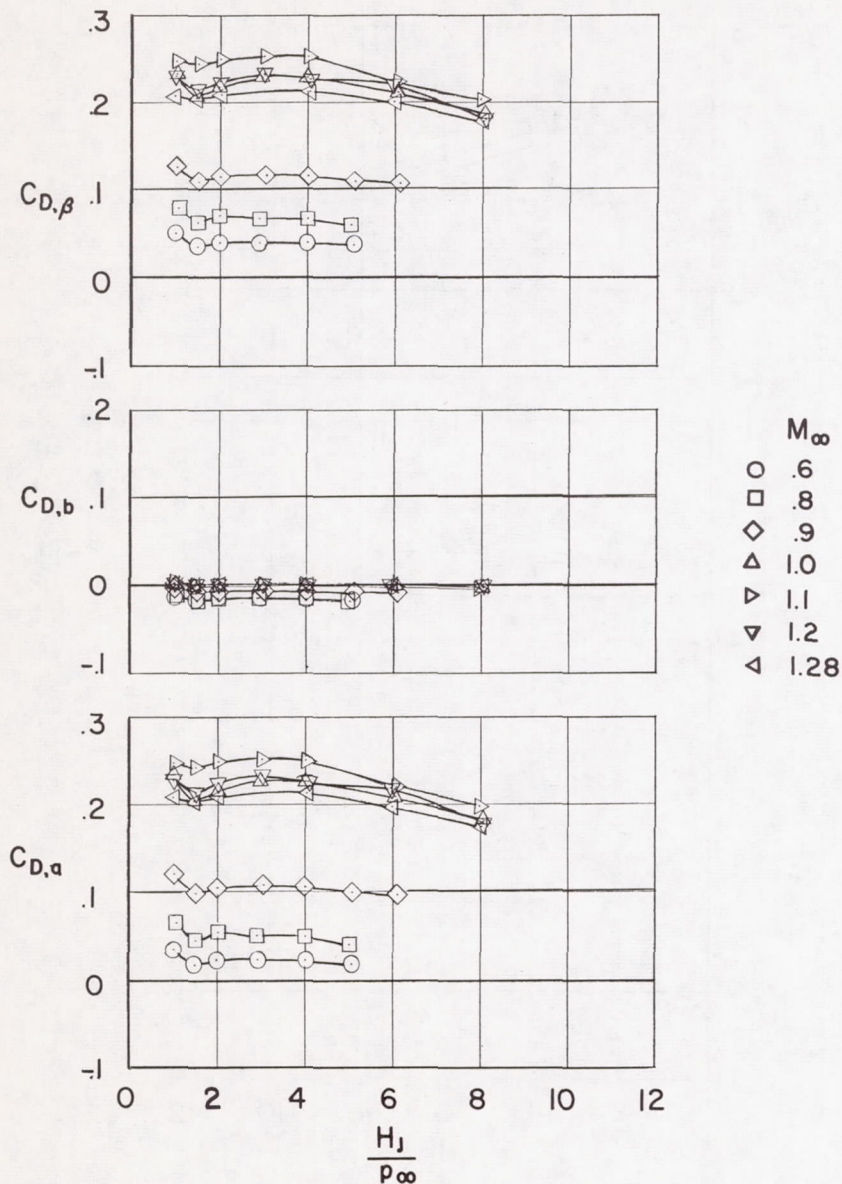
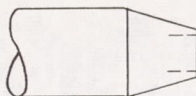
(f) $\beta = 16^\circ$; $d_b/d_m = 0.85$.

Figure 8.- Continued.



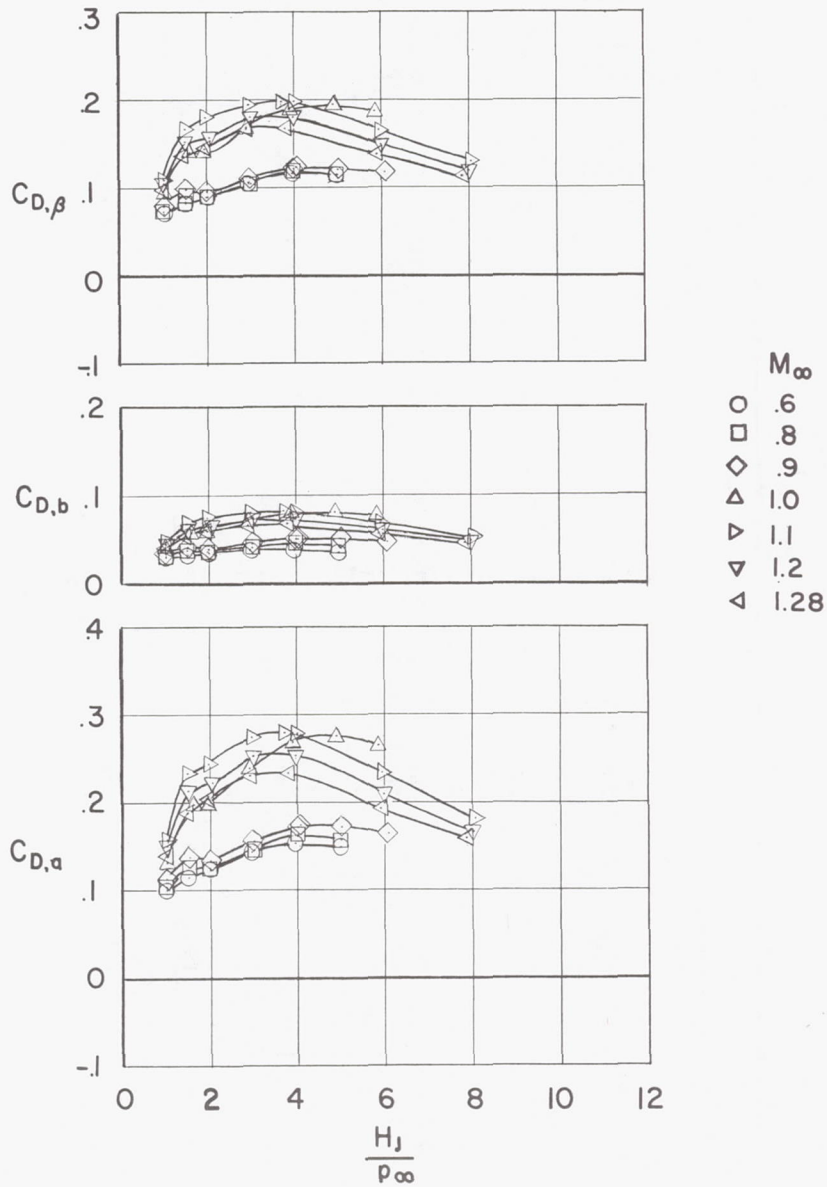
(g) $\beta = 16^\circ$; $d_b/d_m = 0.70$.

Figure 8.- Continued.



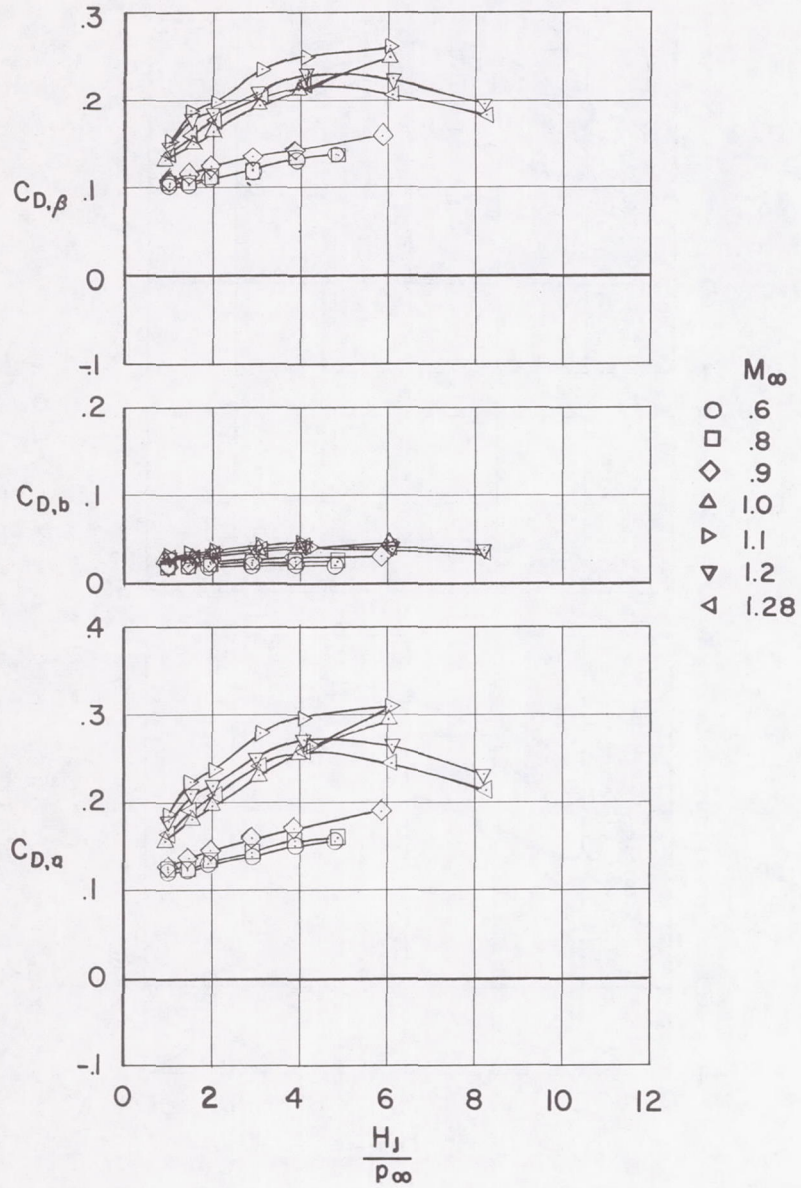
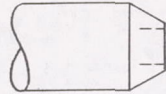
(h) $\beta = 16^\circ$; $d_b/d_m = 0.55$.

Figure 8.- Continued.



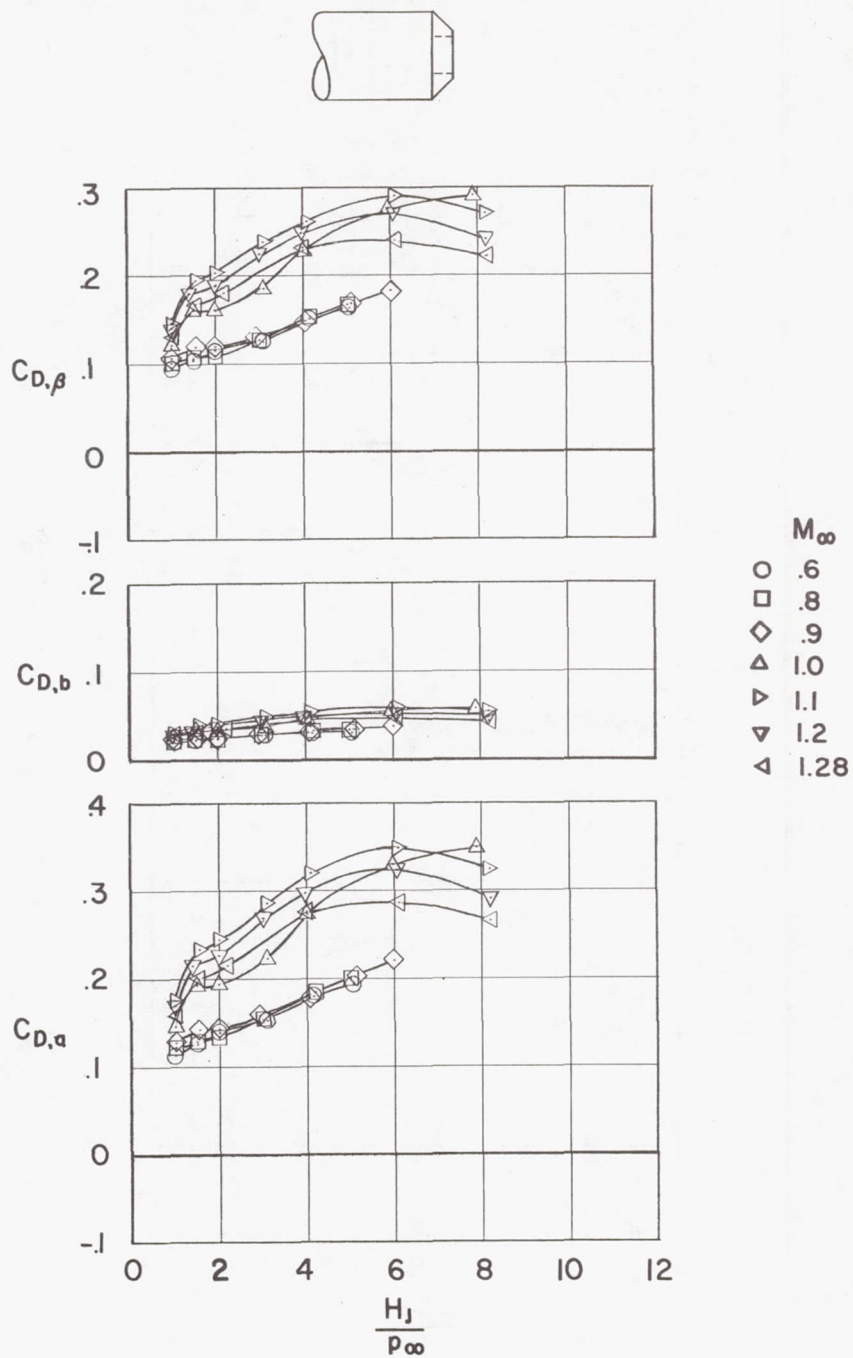
(i) $\beta = 30^\circ$; $d_b/d_m = 0.70$.

Figure 8.- Continued.



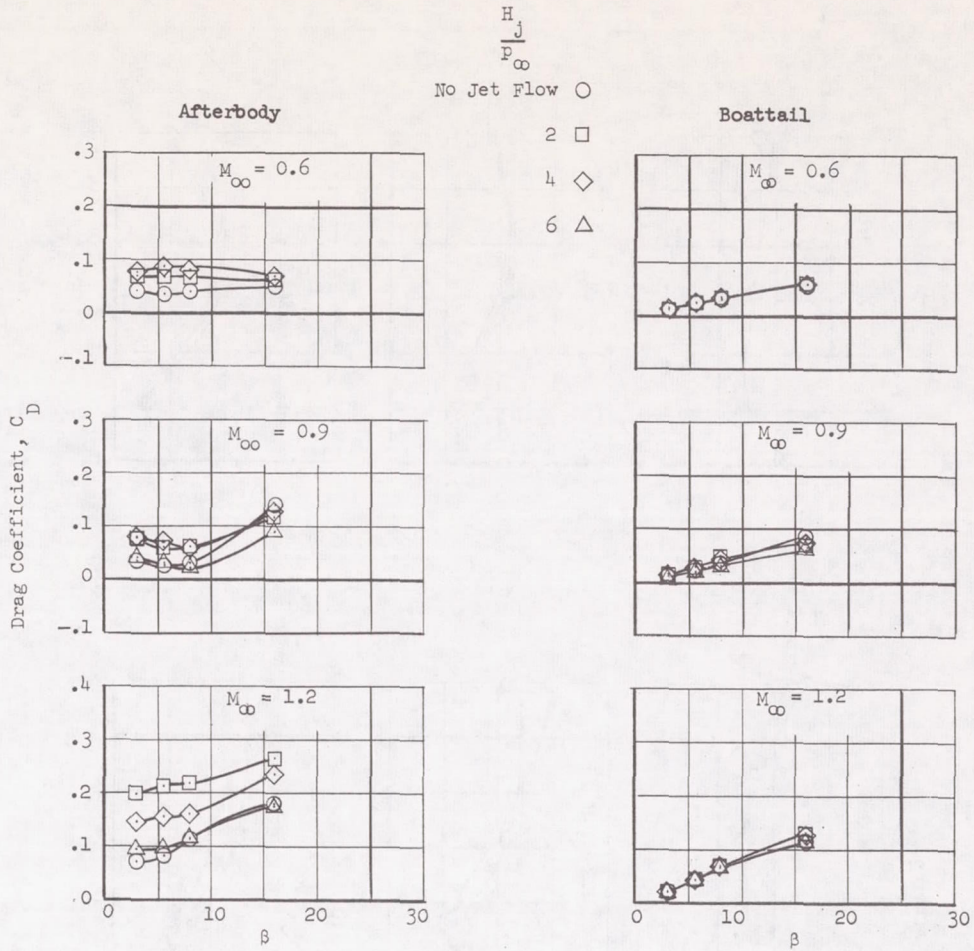
(j) $\beta = 30^\circ$; $d_b/d_m = 0.55$.

Figure 8.- Continued.



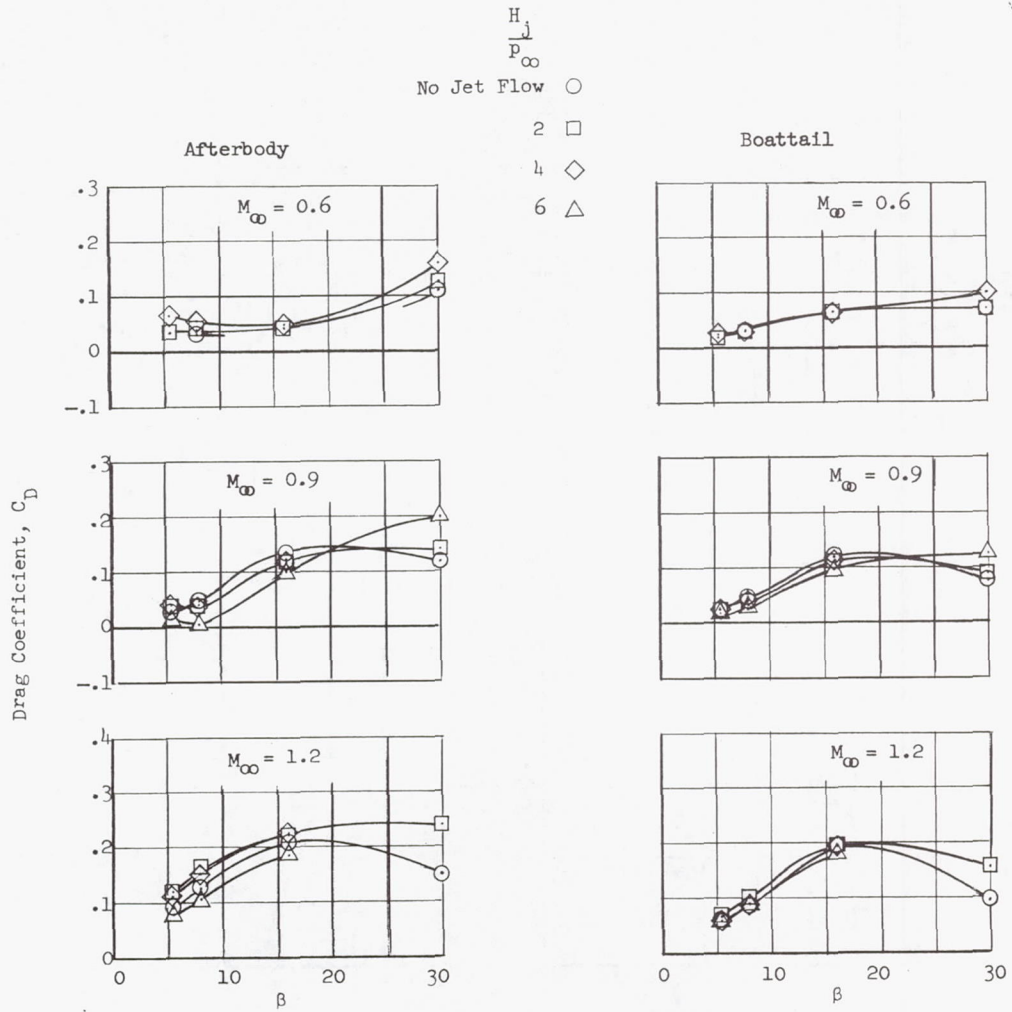
(k) $\beta = 45^\circ$; $d_b/d_m = 0.55$.

Figure 8.- Concluded.



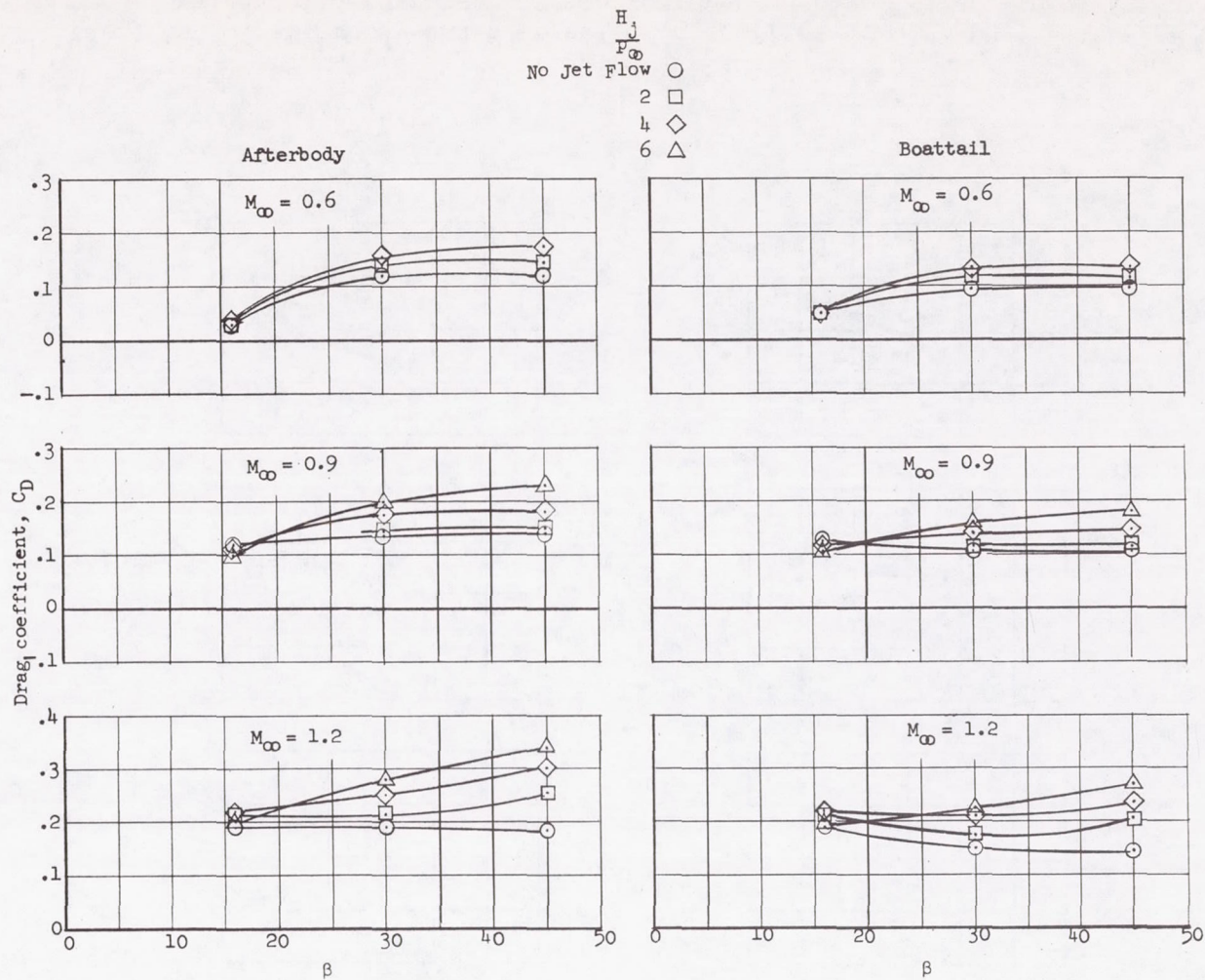
(a) $d_b/d_m = 0.85$.

Figure 9.- Variation of afterbody and boattail drag coefficient with boattail angle at several values of jet pressure ratio and Mach number. $d_j/d_b = 0.65$.



(b) $d_b/d_m = 0.70$.

Figure 9.- Continued.



(c) $d_b/d_m = 0.55$.

Figure 9.- Concluded.

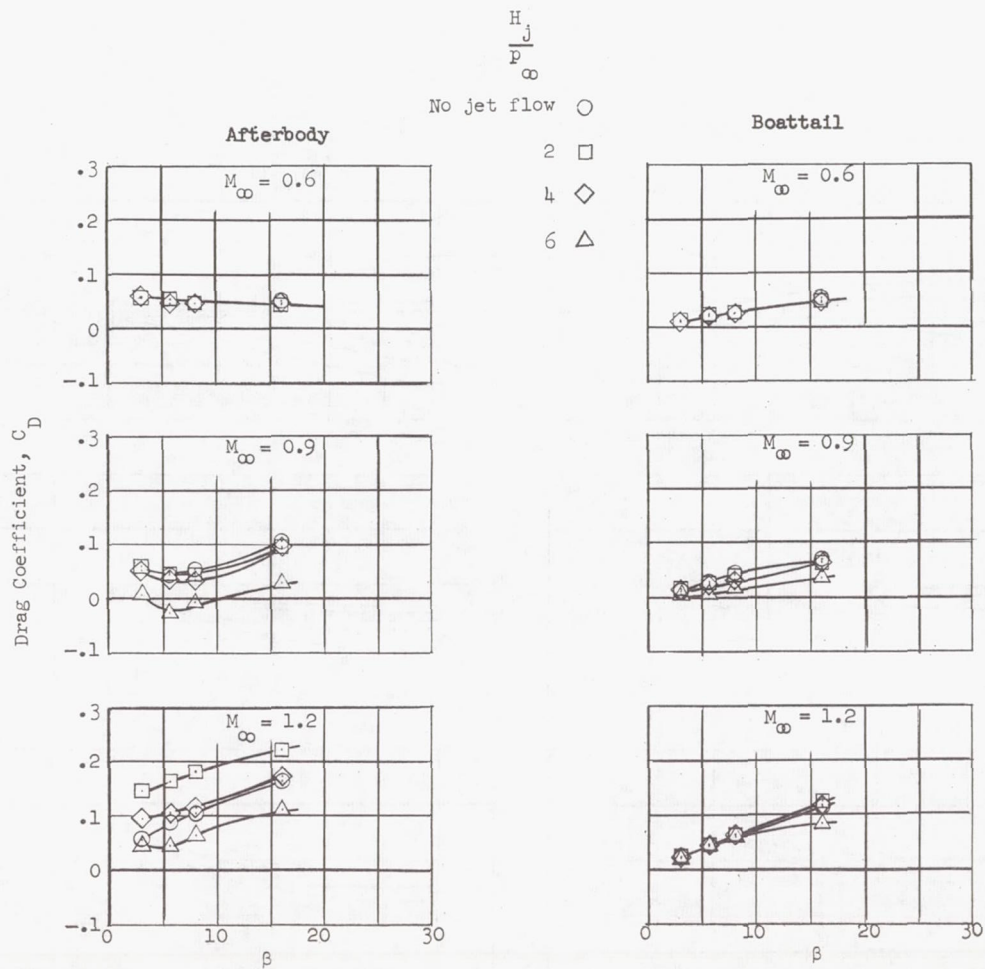
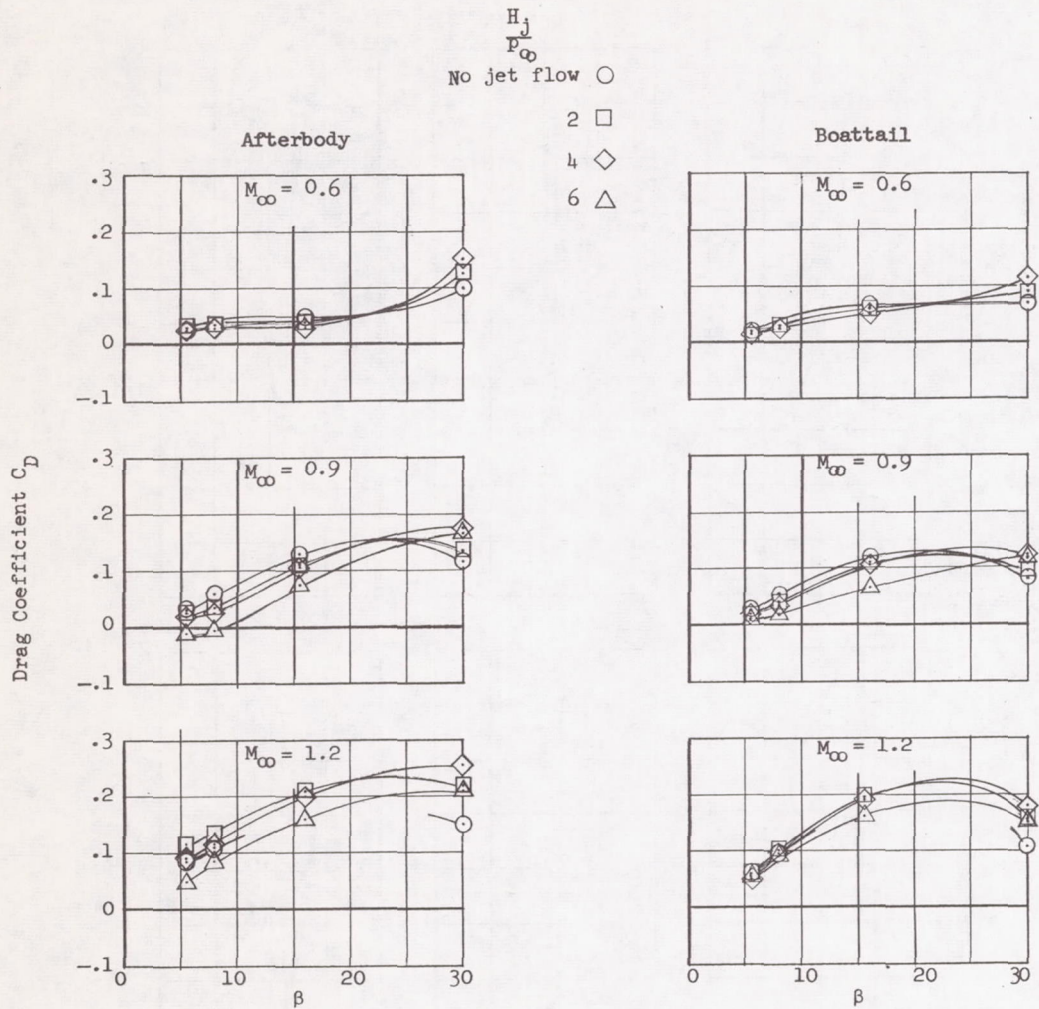
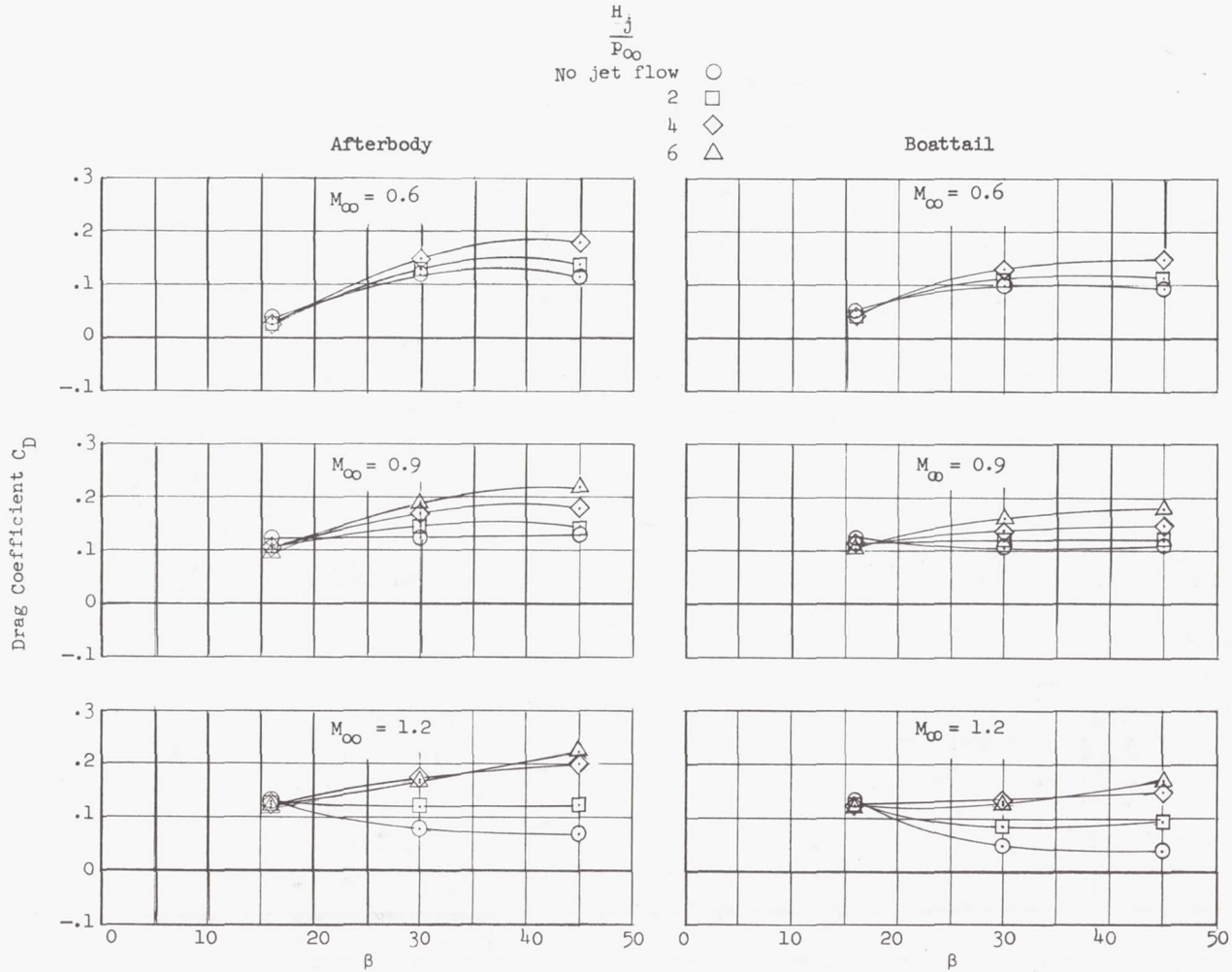


Figure 10.- Variation of afterbody and boattail drag coefficient with boattail angle at several values of jet pressure ratio and Mach number. $d_j/d_b = 0.75$.



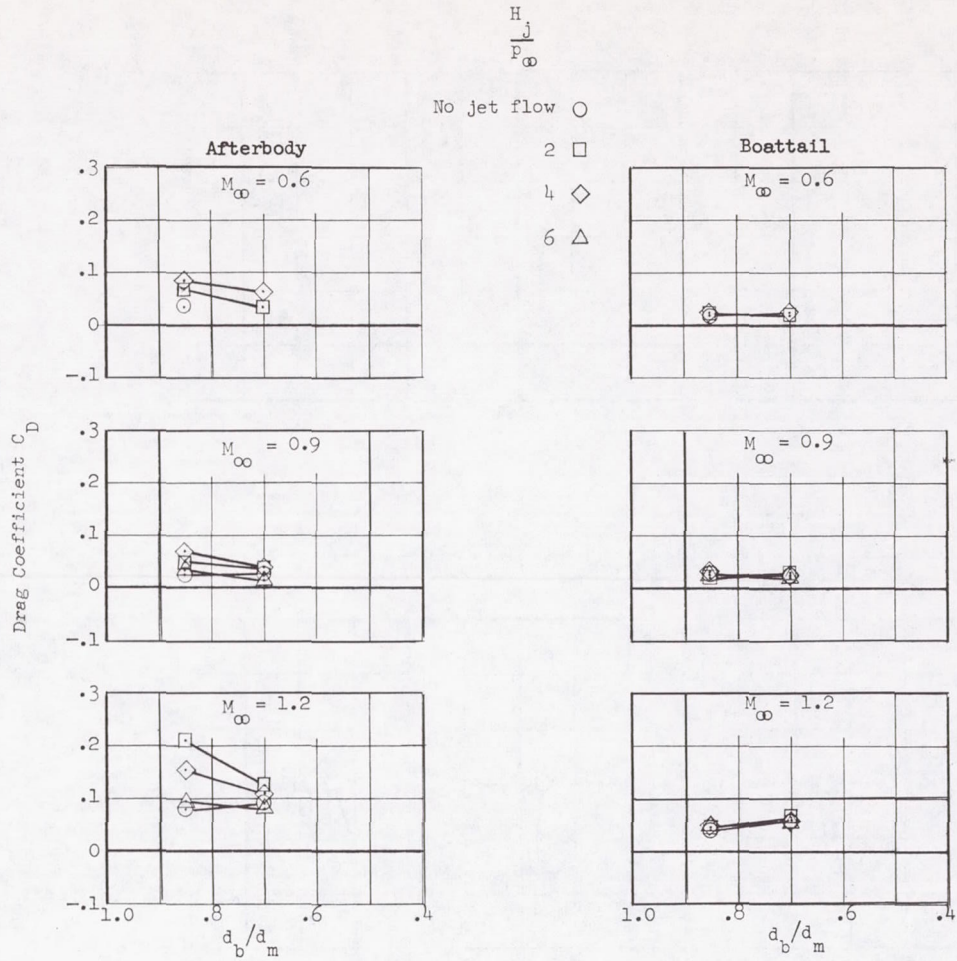
(b) $d_b/d_m = 0.70$.

Figure 10.- Continued.



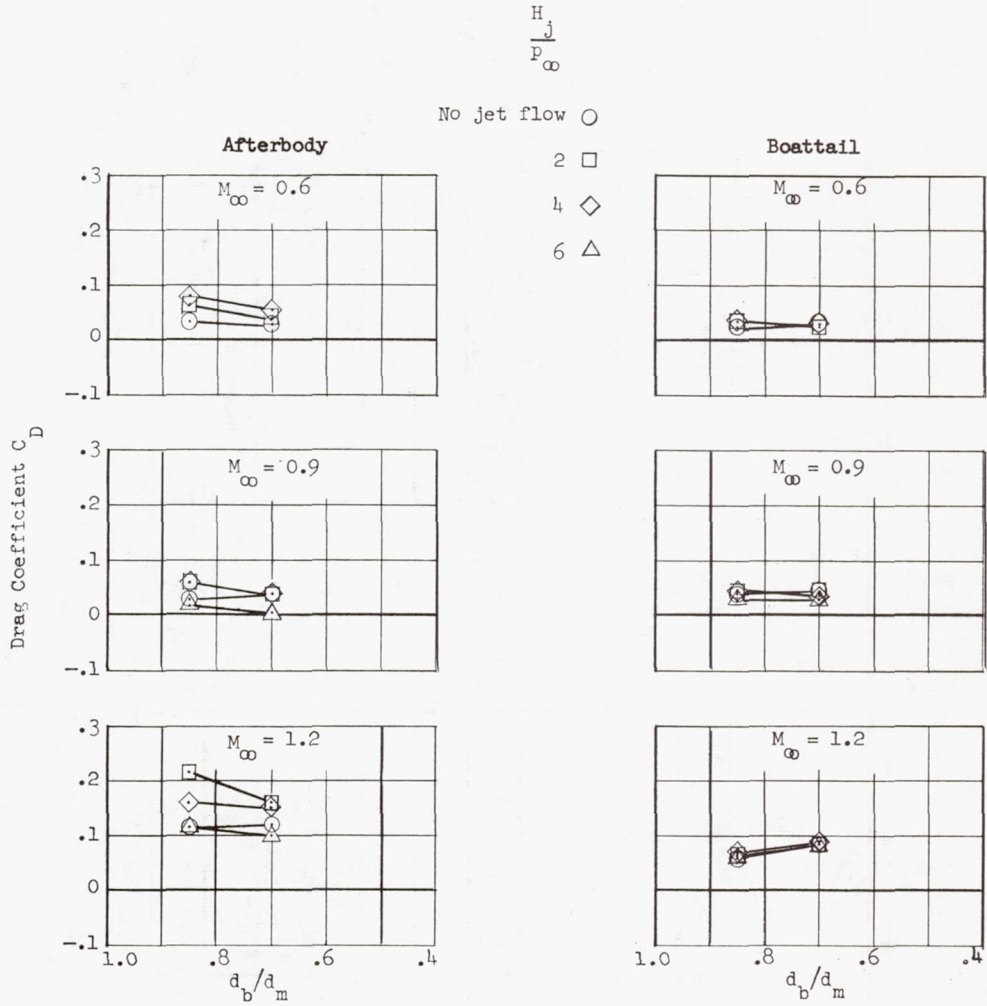
(c) $d_b/d_m = 0.55$.

Figure 10.- Concluded.



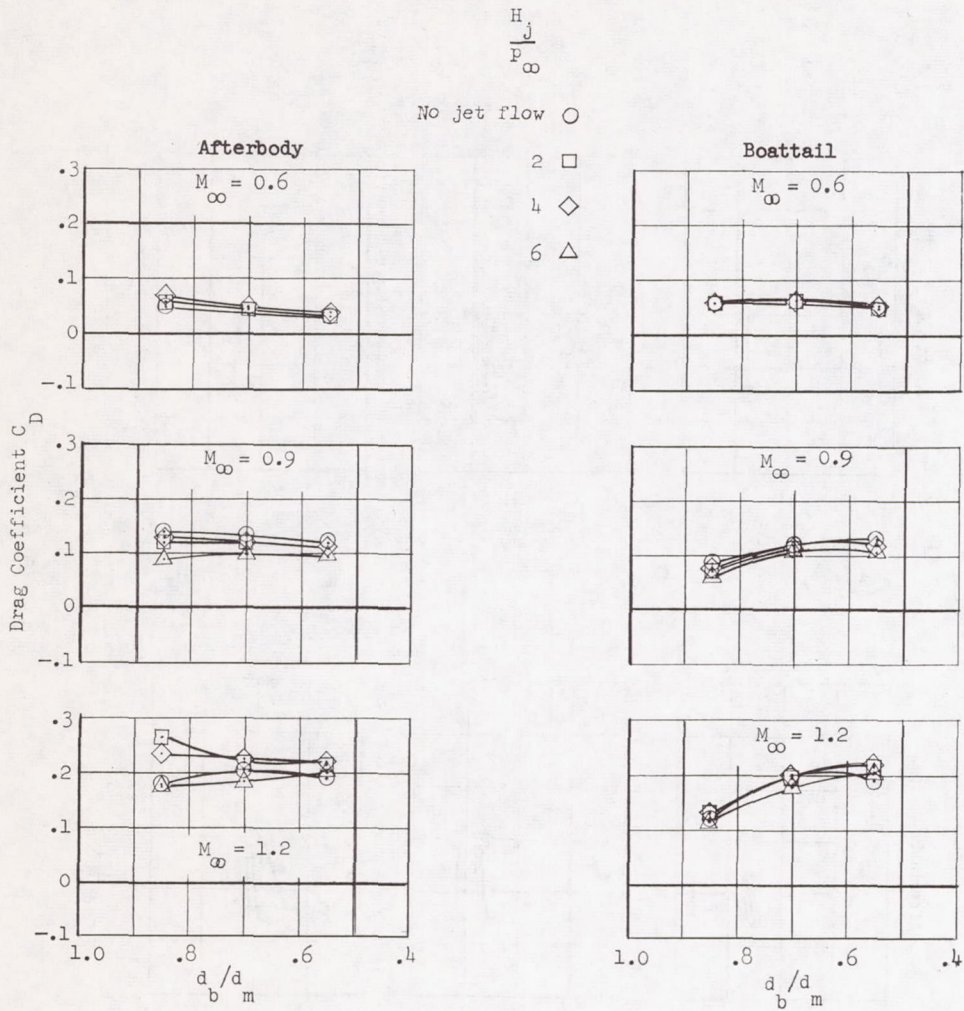
(a) $\beta = 5.6^\circ$.

Figure 11.- Variation of afterbody and boattail drag coefficients with base diameter ratio. $d_j/d_b = 0.65$.



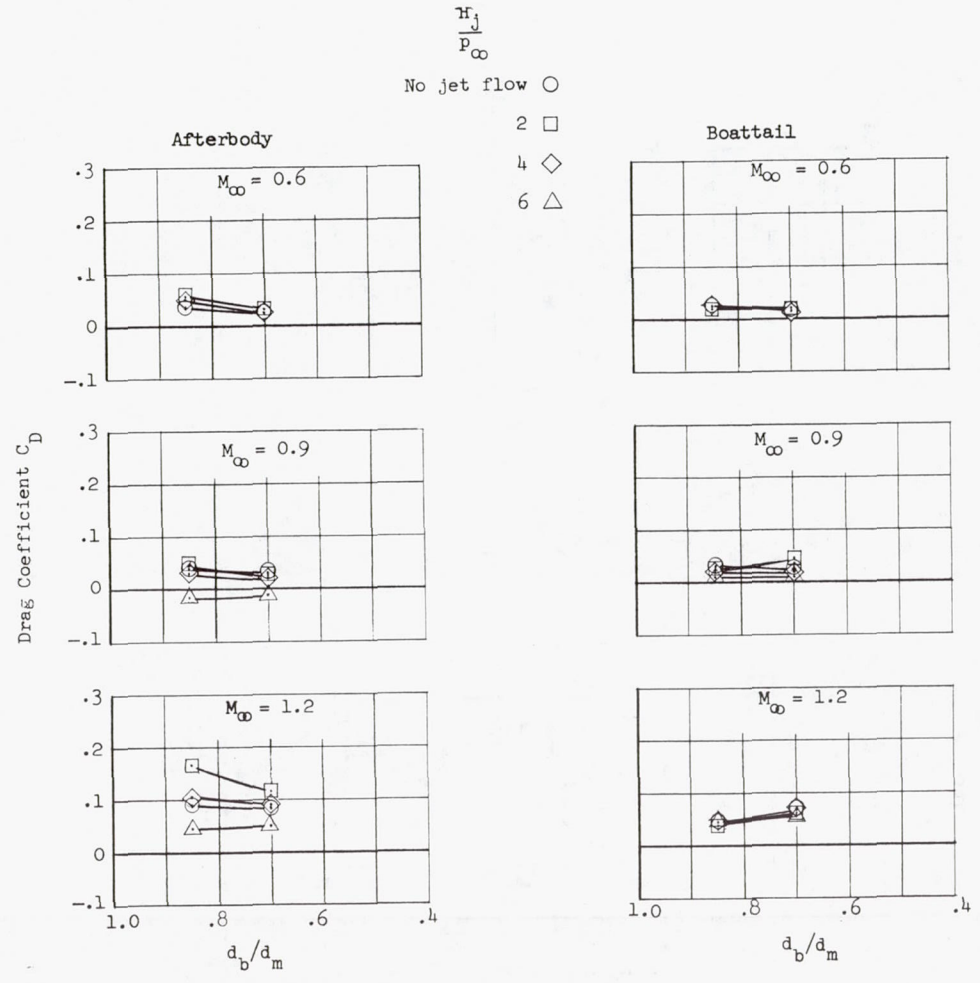
(b) $\beta = 8^\circ$.

Figure 11.- Continued.



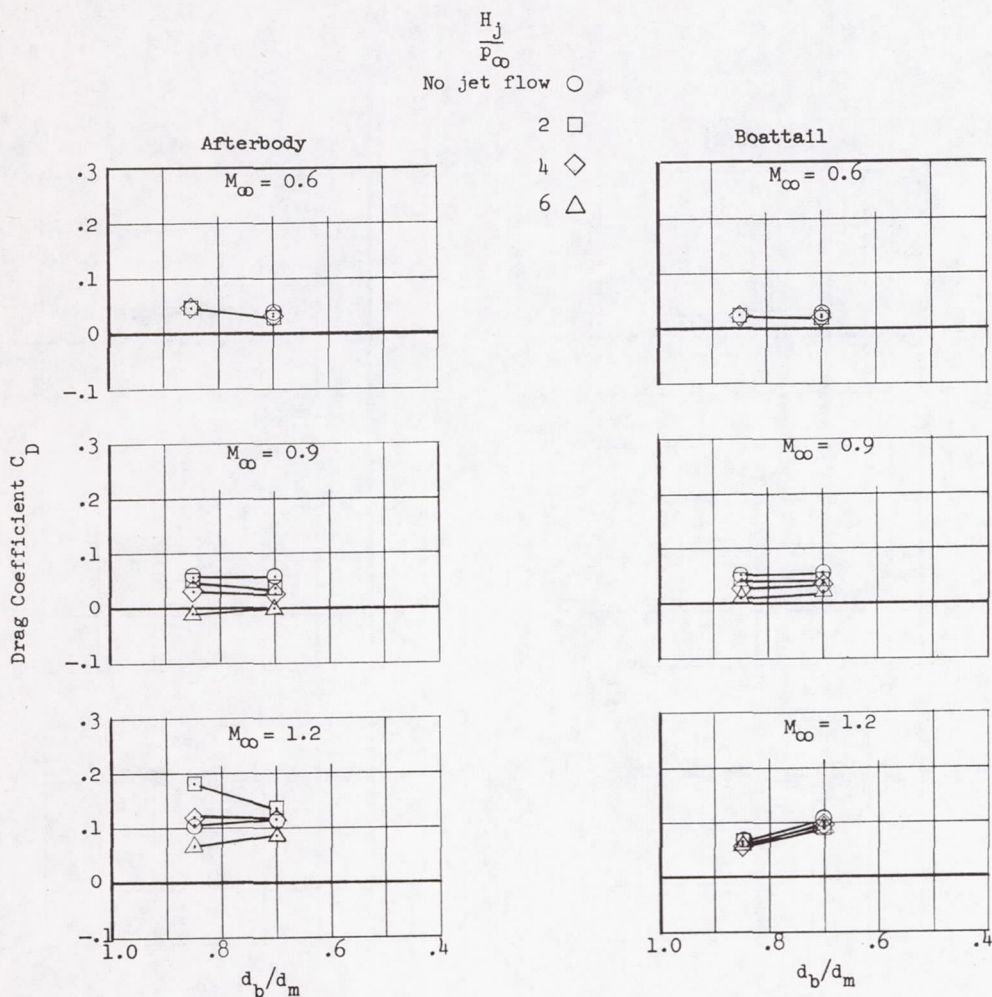
(c) $\beta = 16^\circ$.

Figure 11.- Concluded.



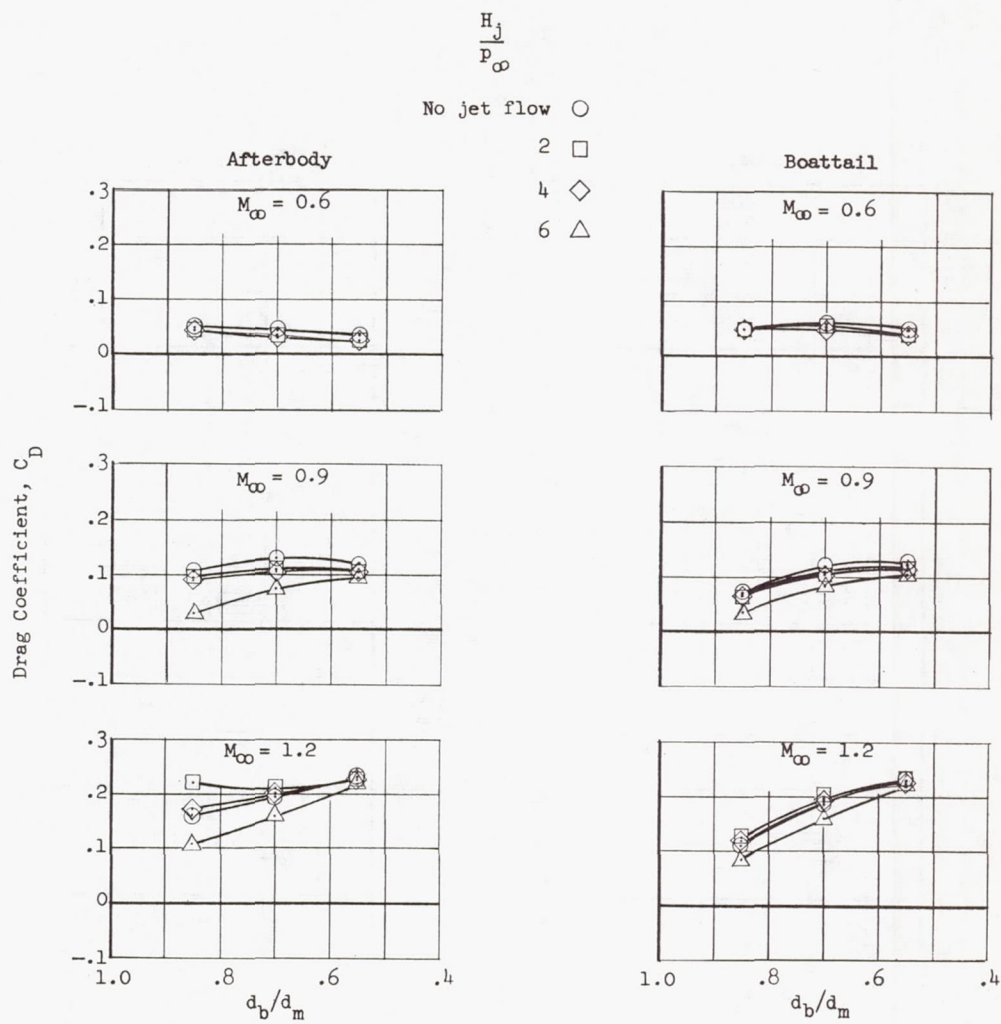
(a) $\beta = 5.6^\circ$.

Figure 12.- Variation of afterbody and boattail drag coefficients with base diameter ratio. $d_j/d_b = 0.75$.



(b) $\beta = 8^\circ$.

Figure 12.- Continued.



(c) $\beta = 16^\circ$.

Figure 12.- Concluded.

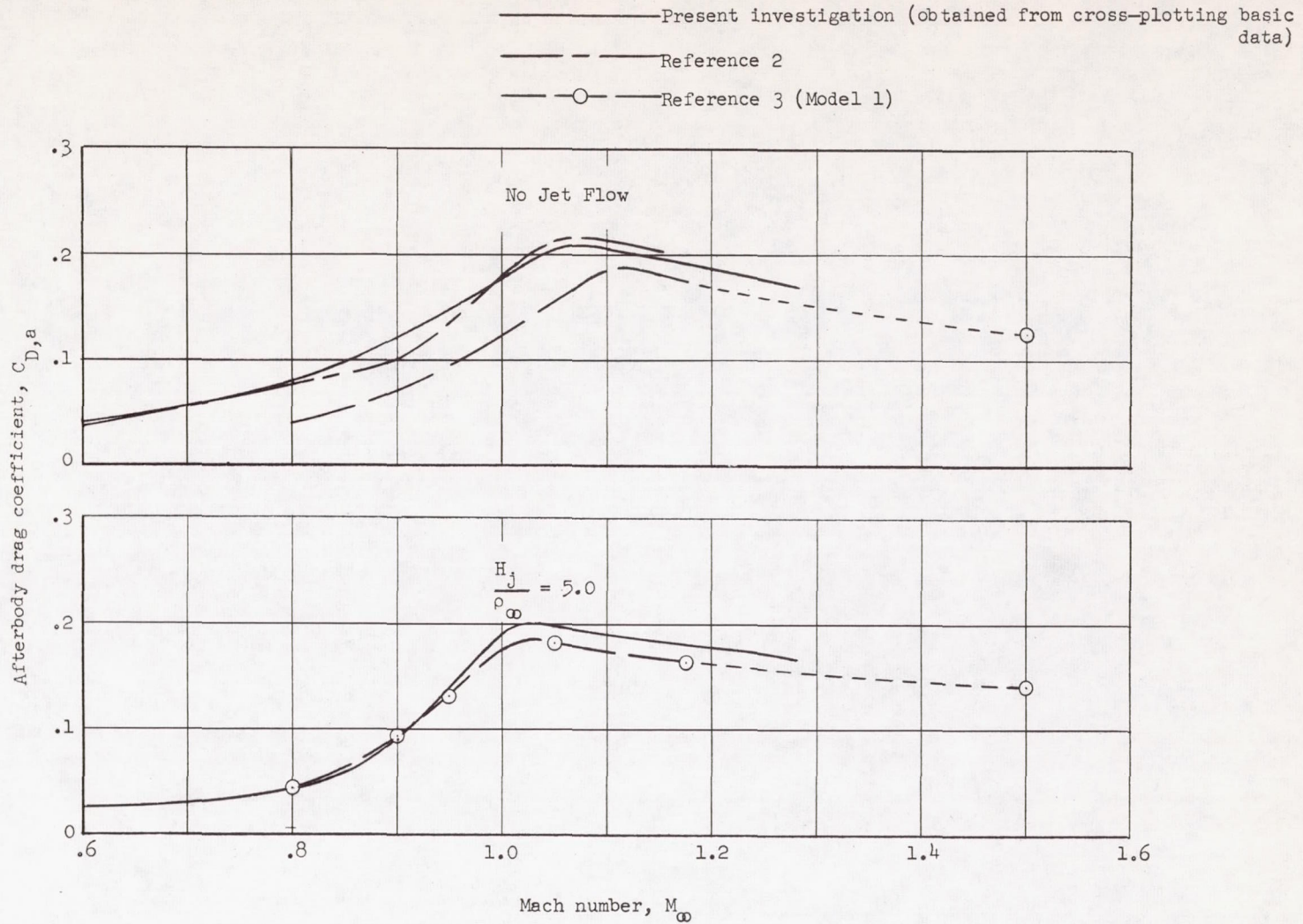


Figure 13.- Comparison of the afterbody drag coefficient of a $\beta = 15^\circ$ afterbody obtained from present data with a similar model from references 2 and 3. $\beta = 15^\circ$; $d_b/d_m = 0.75$; $d_j/d_b = 0.75$.